Università degli Studi di Padova
Dipartimento di Scienze Oncologiche e Chirurgiche

SCUOLA DI DOTTORATO DI RICERCA IN ONCOLOGIA E ONCOLOGIA CHIRURGICA
CICLO XXII

FUNCTIONAL CHARACTERIZATION OF THE p13 PROTEIN OF HTLV-1

Direttore della Scuola: Ch.ma Prof.ssa Paola Zanovello
Supervisore: Dott. Vincenzo Ciminale

Dottoranda: Dott. ssa Roberta Biasiotto

INDEX

ABBREVIATIONS

- APC anaphase promoting complex
- APAF-1 apoptosis protease activating factor-1
- ATLL adult T-cell leukemia-lymphoma
- BLV bovine leukemia virus
- BSA bovine serum albumin
- CA capsid
- CAMK calmodulin-dependent protein kinase
- CBP CREB binding protein
- CDK4 cyclin-dependent kinase 4
- CI colocalization index
- CRAC Ca^{2+}-release-activated Ca^{2+} channel
- CREB cAMP response element binding protein
- CRM1 chromosome region maintenance 1 protein
- CTL cytotoxic T-lymphocyte
- DAG diacylglycerol
- $\Delta\psi$ mitochondrial membrane potential
- DMEM Dulbecco's modified Eagle's medium
- DTT dithiothreitol
- EGTA ethylene glycol tetraacetic acid
- Endo G endonuclease G
- ER endoplasmic reticulum
- FCCP carbonylcyanide p-trifluoromethoxyphenylhydrazone
- FCS fetal calf serum
- FI fluorescence intensity
- FoxP3 Forkhead Box P3
- GSK3β glycogen synthase kinase 3 β
- HBZ HTLV-1 bZIP factor
- hDlg human Disc large
- HBV hepatitis B virus
- HCV hepatitis C virus
- HIV human immunodeficiency virus
- Hsp60 heat shock protein 60
- hTERT human telomerase reverse transcriptase

- HTLV-1 human T-lymphotropic virus type 1
- ICAM-1 intracellular adhesion molecule-1
- IEF isoelectric focusing
- IL-2 interleukin-2
- I-κB inhibitor of NF-κB
- IKKβ I-κB kinase β subunit
- IKKγ I-κB γ subunit
- IMM inner mitochondrial membrane
- IPG immobilized pH gradient
- IP3 inositol 1,4,5-trisphosphate
- KRB Krebs-Ringer Buffer
- Jak Janus associated kinase
- LTR long terminal repeat
- MA matrix
- MES 2-(*N*-morpholino)ethanesulfonic acid
- MHC-I major hystocompability complex I
- MHC-I Hc MHC class I heavy chain
- MTOC microtubule-organizing center
- MTS mitochondrial targeting signal
- NC nucleocapsid
- NCX Na^{+}/Ca^{2+} exchanger
- NK natural killer cells
- NLS nuclear localization signal
- NFAT nuclear factor of activated T-cells
- NF-κB nuclear factor kappa-light chain-enhancer of activated B-cells
- Omi/HtrA2 Omi stress-regulated endoprotease/high temperature requirement protein A2
- ORF open reading frame
- PBMC peripheral blood mononuclear cells
- PBS phosphate-buffered saline
- pI isoelectric point
- PKA protein kinase A
- PKC protein kinase C
- PMCA plasma membrane Ca^{2+}-ATPase

- PS phosphatidylserine
- PTP permeability transition pore
- PVDF polyvinylidene fluoride
- RaM rapid uptake mode
- ROS reactive oxygen species
- RT reverse transcriptase
- RxRE Rex-responsive element
- ROC receptor-operated Ca^{2+} channel
- RPMI Roswell Park Memorial Institute
- SDS sodium dodecyl sulphate
- SDS-PAGE sodium dodecyl sulphate - polyacrylamide gel electrophoresis
- SH3 Src-homology 3
- Smac/DIABLO second mitochondria-derived activator of caspase/direct inhibitor of apoptosis protein (IAP)-binding protein with low pI
- SOC store-operated Ca^{2+} channel
- SOCE store-operated Ca^{2+} entry
- SMOC second messenger-operated Ca^{2+} channel
- SRF serum responsive factor
- STAT-5 signal transducers and activators of transcription-5
- STLV simian T-lymphotropic virus
- TCR T-cell receptor
- TES N-tris-(hydroxymethyl)methyl-2-aminoethanesulphonic acid
- TLR4 toll-like receptor 4
- TMR tetramethyl rhodamine
- TMRM tetramethyl rhodamine methyl ester
- TPA 12-O-Tetradecanoylphorbol-13-acetate
- TRE Tax-responsive element
- TSP/HAM tropical spastic paraparesis/human T-cell leukemia virus-1-associated myelopathy
- VDAC voltage-dependent anionic channel
- VOC voltage-operated Ca^{2+} channel
-WB western blot

ABSTRACT

HTLV-1 is the causative agent of adult T-cell leukemia-lymphoma (ATLL), an aggressive neoplasm of mature CD4+ T cells refractory to current therapies, and of HAM/TSP, a neurodegenerative disease. HTLV-1 is a complex retrovirus whose genome encodes several regulatory and accessory proteins (Rex, Tax, HBZ, p12, p30, p13) in addition to the structural proteins (gag, pol, env) common to all retroviruses.

Previous studies demonstrated that HTLV-1 p13, an 87-amino acid protein, is targeted to the inner membrane of mitochondria and induces mitochondrial fragmentation. *In vitro* studies carried out using the full-length synthetic protein and isolated mitochondria showed that p13 induces a potential-dependent potassium (K^+) influx into the mitochondrial matrix, accompanied by a dose-dependent depolarization, and reduces the threshold for permeability transition pore (PTP) opening. This effect on K^+ permeability is mediated by an amphipatic α-helical domain (amino acids 21-30), in which four positively charged arginines play a key role. p13 slows down cell proliferation, promotes apoptosis triggered by ceramide and Fas L, and interferes with tumor growth in experimental models.

The studies described in the present thesis were aimed at testing the effects of p13 on mitochondria in living cells. Using the potential-dependent probe tetramethyl rhodamine methyl ester (TMRM), we demonstrated that p13 induces dose-dependent mitochondrial depolarization of HeLa cells. The p13RQ mutant, which is inactive on K^+ permeability, had no effect on mitochondrial membrane potential ($\Delta\psi$). Similar results were obtained with Jurkat T-cells. As $\Delta\psi$ is a key factor controlling mitochondrial calcium (Ca^{2+}) uptake, we analyzed the effect of p13 on Ca^{2+} homeostasis. To this end, we employed organelle-targeted aequorin and showed that p13 specifically reduced mitochondrial Ca^{2+} uptake, upon histamine stimulation, while it does not alter Ca^{2+} concentration in the cytoplasm or the endoplasmic reticulum (ER). This effect suggests that p13 might control key processes regulated through Ca^{2+} signalling, such as T-cell activation and death.

The observation that p13's effect on $\Delta\psi$ was heterogeneous at intermediate levels of expression suggested the existence of mechanisms regulating p13 function. In the present study, we investigated the possible role of phosphorylation in the regulation of p13 function. In particular, we focused on serine 15 (S15), a putative protein

kinase C (PKC) phosphorylation site located in the proximity of the α-helical domain. *In vitro* phosphorylation assays on $p13_{[9-22]}$ and $p13S15A_{[9-22]}$ synthetic peptides confirmed the phosphorylation of S15 by purified PKC and by cytosolic and mitochondrial lysates from Jurkat T-cells as a source of kinases. We also confirmed the *in vitro* phosphorylation of the full-length synthetic p13 by Jurkat T-cell lysates. Preliminary results obtained by 2D-electrophoresis analysis of Jurkat T-cells transiently transfected with p13 demonstrated that the protein is detected in two main forms differing in their pI. We then analyzed the functional effects of S15 phosphorylation by producing the phosphoablative (p13S15A) and phosphomimetic (p13S15D) mutants and studying their properties in HeLa cells. Results demonstrated that the presence of a negative charge on residue 15 enhances the effect of p13 on the induction of mitochondrial fragmentation. Interestingly, using TMRM, we found that the phosphomimetic mutant induces mitochondrial depolarization at much lower level of expression, compared to p13 wild-type. Taken together, these results suggest that phosphorylation on S15 might influence the biological properties of p13, and open the door to future studies of this and other cellular mechanisms regulating p13 function.

RIASSUNTO

Il virus T-linfotropico umano di tipo 1 (HTLV-1) è associato all'insorgenza della leucemia-linfoma a cellule T dell'adulto (ATLL), un'aggressiva neoplasia dei linfociti T CD4+ maturi, e della mielopatia associata ad HTLV-1/paraparesi spastica tropicale (HAM/TSP), una patologia degenerativa del sistema nervoso centrale. HTLV-1 è classificato come retrovirus complesso in quanto il suo genoma codifica, oltre a proteine strutturali (gag, env, pol), anche proteine regolatorie (Tax e Rex) ed accessorie (p30, p12, p13, HBZ), dalla funzione ancora non del tutto chiarita.

Precedentemente è stato dimostrato che la proteina accessoria p13 (la cui sequenza è costituita da 87 aminoacidi) si localizza nella membrana mitocondriale interna ed induce marcata frammentazione di questi organelli. Mediante studi *in vitro* condotti con p13 sintetica e mitocondri isolati è stato dimostrato che p13 induce un influsso di potassio (K^+) potenziale-dipendente all'interno della matrice mitocondriale. L'alterazione della permeabilità mitocondriale indotta da p13 è accompagnata da una depolarizzazione dose-dipendente e da una riduzione della soglia di apertura del poro di transizione della permeabilità mitocondriale (PTP). L'influsso di K^+ è dovuto alla presenza di un dominio anfipatico ad α-elica (tra gli aminoacidi in posizione 21 e 30), in cui le quattro arginine in posizione 22, 25, 29 e 30 svolgono un ruolo fondamentale per la funzione di p13. p13 rallenta la proliferazione cellulare, promuove l'apoptosi mediata da ceramide e Fas L e interferisce con la crescita tumorale in modelli sperimentali *in vivo*.

Gli studi descritti nella presente tesi sono stati mirati alla analisi degli effetti di p13 a livello mitocondriale in cellule vitali. Usando la sonda potenziale-dipendente tetrametil-rodamina-metil-estere (TMRM), è stato dimostrato che p13 induce una depolarizzazione mitocondriale dose-dipendente in cellule HeLa. Il mutante p13RQ, che non altera la permeabilità della membrana interna al K^+, non ha evidenziato effetti a livello del potenziale di membrana mitocondriale ($\Delta\psi$). Risultati analoghi sono stati ottenuti utilizzando cellule T come modello cellulare.

Dato che il $\Delta\psi$ è fondamentale nel controllo dell'ingresso di calcio (Ca^{2+}) nel mitocondrio, abbiamo analizzati gli effetti di p13 nell'omeostasi del Ca^{2+}.

A tal fine abbiamo utilizzato la sonda Ca^{2+}-sensibile equorina, specifica per dati compartimenti cellulari. I risultati di questa analisi hanno evidenziato che, in seguito a stimolazione con istamina, l'influsso mitocondriale di Ca^{2+} risulta ridotto in

presenza di p13, che invece non induce alterazioni nella concentrazione di Ca^{2+} del citoplasma e del reticolo endoplasmatico. Questo effetto suggerisce che p13 potrebbe controllare fondamentali processi, regolati da Ca^{2+}, come l'attivazione e la morte delle cellule T.

L'osservazione dell' eterogeneità dell' effetto di p13 sul $\Delta\psi$, a livelli intermedi di espressione, ha suggerito l'esistenza di meccanismi preposti alla regolazione della funzione della proteina. Abbiamo quindi analizzato il ruolo della fosforilazione come possibile evento regolativo della funzione di p13. In particolare, è stata individuata la serina in posizione 15 come possibile sito di fosforilazione da parte di protein-chinasi C (PKC). S15 potrebbe essere un sito chiave per la regolazione della funzione di p13 poiché è localizzata vicino al dominio funzionale ad α-elica, responsabile dell'influsso di K^+ nella matrice mitocondriale. Saggi di fosforilazione *in vitro* condotti sui peptidi sintetici $p13_{[9-22]}$ e $p13S15A_{[9-22]}$ hanno confermato la fosforilazione di S15 da parte di lisati cellulari (mitocondriale e citosolico) di cellule T Jurkat, oltre che da parte di una miscela commerciale di PKC, come fonte di chinasi. La reazione di fosforilazione *in vitro* da parte di lisati cellulari è stata anche confermata sulla proteina sintetica $p13_{[1-87]}$. Risultati preliminari ottenuti mediante esperimenti di elettroforesi bidimensionale di lisati di cellule T Jurkat trasfettate transientemente con p13 hanno dimostrato che la proteina, espressa in cellule T, esiste in due forme principali, che differiscono per punto isoelettrico (pI). Sono stati inoltre analizzati gli effetti funzionali della fosforilazione di S15 producendo dei mutanti fosfomimetico (p13S1D) e fosfoablativo (p13S15A) e studiando le loro proprietà in cellule HeLa. I risultati di questi studi hanno evidenziato che la presenza della carica negativa nel residuo 15 rafforza gli effetti di p13 nell'induzione della frammentazione mitocondriale. Mediante saggi di incubazione con TMRM è stato dimostrato che il mutante fosfomimetico induce depolarizzazione mitocondriale ad un livello di espressione inferiore rispetto alla proteina *wild-type*. Complessivamente, questi risultati suggeriscono che la fosforilazione in S15 possa influenzare le proprietà biologiche di p13. Questo studio apre la strada ad ulteriori indagini, finalizzate all'analisi di questo e di altri meccanismi alla base della regolazione della funzione di p13.

1 INTRODUCTION

1.1 Human T-lymphotropic virus type 1: epidemiology, pathogenesis, and taxonomy

Human T-Lymphotropic virus type 1 (HTLV-1) is the first isolated human retrovirus with established oncogenic properties (Hinuma et al., 1981; Poiesz et al., 1980). HTLV-1 infects about 20 million people worldwide and is endemic in south-western Japan, Central Africa, and the Caribbean basin, Central and South America, and Melanesian Islands. Sporadic infection occurs in Europe and North America. Transmission of the virus may occur in a “vertical” manner from mother to newborn (e.g. through breastfeeding), or “horizontally” through exchange of biological fluids (e.g. blood and semen) (Proietti et al., 2005). HTLV-1 is the causative agent of two distinct pathologies, adult T-cell leukemia/lymphoma (ATLL), an aggressive malignancy of mature CD4+ T-cells that is extremely refractory to current therapies (Tsukasaki et al., 2009; Uchiyama et al., 1977), and HTLV-1-associated myelopathy/tropical spastic paraparesis (HAM/TSP), a demyelinating neurodegenerative disease (Gessain et al., 1985; Osame et al., 1986). In addition, accumulating evidence supports an association between HTLV-1 infection and a number of chronic inflammatory diseases such as arthropathy and uveitis (Mochizuki et al., 1996; Sato et al., 1991).

The majority of HTLV-1-infected individuals remain asymptomatic throughout life; only 2-5% develop ATLL or HAM/TSP after a latency period of decades or several years, respectively (Kawano et al., 1985).

ATLL is classified into four clinical forms: acute, lymphoma, chronic, and smouldering types (Tsukasaki et al., 2009). In some cases the acute phase of ATLL is preceded by peripheral lymphocytosis characterized by poly- or oligoclonal integration of the viral genome. Acute ATLL is characterized by the presence of a dominant leukemic clone with monoclonal integration of the provirus. These cells are characterized by multi-lobulated nuclei and are called "flower cells". ATLL cells are usually CD3+ CD4+ CD8- CD25+ and frequently accumulate in peripheral blood as well as in lymphoid organs and skin. A study reported that 10 out of 17 ATLL cases (59%) espressed Forkhead Box P3 (FoxP3), whose expression is characteristic of regulatory T cells (T_{reg} cells), and that ATLL cells can suppress the proliferation of bystander CD4+ T-lmphocytes, suggesting that some cases of ATLL originate

from virus-infected T_{reg} cells (Karube et al., 2004). The severe immunodeficiency and the opportunistic infections that occur in ATLL patients could thus depend in part on the immunosoppressive properties of ATLL T_{reg} cells. Furthermore, a recent study demonstrated that HTLV-1 infection is associated with an abnormal FoxP3 expression in CD4+ circulating cells and that, *in vivo*, the frequency of CD4+ FoxP3+ Tax- cells negatively correlates with the immunosurveillance of infected cells mediated by CD8+ T-lymphocytes (Toulza et al., 2008). One of the most common characteristics of ATLL is hypercalcemia, which results from the transcriptional activation of a parathormone-like peptide induced by the viral Tax protein.

HAM/TSP is characterized by a slowly progressive spastic paraparesis, associated with bladder dysfunction and sensory disorders (Rodgers, 1965). Parenchymal and perivascular infiltration of mononuclear cells occurs in the white and gray matter of the spinal cord, resulting in demyelination and fibrosis (Iwasaki, 1990). The presence of infiltrating T-cells in the spinal cord lesions and of Tax-specific cytotoxic T-lymphocytes (CTL) in the cerebrospinal fluid and in the peripheral blood mononuclear cells suggests that HAM/TSP might have an autoimmune base (Osame, 2002; Verdonck et al., 2007). This hypothesis is consistent with the association between HLA haplotype and the risk of developing HAM/TSP (Barmak et al., 2003).

HTLV-1 belongs to the Retroviridae family, Oncovirinae sub-family, Deltaretrovirus genus, which also includes HTLV-2, -3, -4, simian T-lymphotropic virus (STLV), and bovine leukemia virus (BLV). STLV and BLV infections are associated with neoplastic diseases, while the pathogenicity of HTLV-2, -3, -4 has not been clearly established. (Araujo and Hall, 2004; Feuer and Green, 2005; Mahieux and Gessain, 2009).

It was demonstrated that HTLV-1 infection of peripheral blood mononuclear cells (PBMC) leads to cell immortalization, i.e. the capability to divide indefinitely in an interleukin-2 (IL-2)-independent manner. After several months of culture it is usually possible to detect a mono- or oligoclonal profile of provirus integration as a result of a process that selects for one or few clones that carry several genetic alterations and acquire the capability to grow in an IL-2-independent manner, a hallmark of the transformed phenotype. These cells usually show a CD3+ CD4+ IL-2R+ (interleukin-2 receptor) phenotype, or, rarely, CD3+ CD8+ IL-2R+ (Green and Chen, 2001). The transformed clones express low levels of viral proteins, suggesting that in

this stage the neoplastic phenotype is maintained through a mechanism that is largely independent of viral expression. Silencing of viral gene expression was shown to be due to viral promoter methylation, or accumulation of mutations in tax gene, or deletions of the proviral 5' LTR (Miyazaki et al., 2007; Takeda et al., 2004). The dynamics of infection and immortalization observed *in vitro* recapitulate at least part of the natural hystory of ATLL *in vivo*. Furthermore, ATLL cells also express very little, if any, viral proteins and frequently carry defective proviral copies integrated in the host genome. The propagation and the persistence of the infected cells in the host relies on both *de novo* infection of new host cells and, mainly, through "mitotic transmission" of the integrated viral genome to daughter cells (Overbaugh and Bangham, 2001).

1.2 Infection and virus propagation

The HTLV-1 virion consists of a viral core that contains the viral-encoded enzymes (reverse transcriptase, integrase) and the single-stranded diploid RNA genome surrounded by capsid proteins. A lipoproteic envelope, composed of a plasma membrane-derived lipid bilayer enriched in gp21 and gp46 glycoproteins, surrounds the viral core (Figure 1) (Lairmore and Franchini, 2007; Manel et al., 2005). HTLV-1 presents a broad cell tropism *in vitro* (monocyte and microglial cells, epithelial cells, B- and T- lymphocytes), but *in vivo* it is mainly detected in CD4+ T-lymphocytes (Manel et al., 2005). Efficient viral spread requires direct cell-to-cell contact and is mediated through the interaction between the viral envelope protein gp46 and the glucose transporter GLUT-1 (Manel et al., 2003). Consequently, glucose consumption of the infected target cell is inhibited and extracellular milieau acidification is reduced, possibly causing metabolic alterations that might contribute to the restricted *in vivo* tropism to CD4+ T-cells (Manel et al., 2005; Manel et al., 2003). Proteins that mediate antigen recognition and cell adhesion (e.g. hDlg, neuropilin-1, heparan sulphate proteoglycans) also contribute to HTLV-1 binding and entry into the target cell, and are part of the "virological synapse" (Blot et al., 2004; Ghez et al., 2006; Pinon et al., 2003). The virological synapse is an organized contact area formed following the envelope protein-GLUT1 interaction and gp21-mediated fusion of the cellular membrane. Its assembly results from the polarization of the cytoskeleton of the infected cell and the accumulation of HTLV-1 core complexes and the HTLV-1 genome at the cell junction, from which they are then

transferred to the uninfected cell (Igakura et al., 2003) as enveloped particles (Majorovits et al., 2008). Interestingly, mitochondria also polarize to the virological synapse (Majorovits et al., 2008). The microtubule-organizing center (MTOC) polarization is induced by the engagement of intracellular adhesion molecule-1 (ICAM-1) (Barnard et al., 2005) and activation of the Ras-MEK-ERK pathway (Nejmeddine et al., 2009). Tax is involved in the formation of the virological synapse: it localizes in the contact region between infected and target cells (Nejmeddine et al., 2005) and enhances MTOC formation by stimulating the CREB pathway (Nejmeddine et al., 2005; Nejmeddine et al., 2009). Another mode of HTLV-1 transmission is mediated through an extracellular biofilm-like structure that stores viral particles, facilitating virus spread after cell-to-cell contact (Pais-Correia et al., 2010). Both the virological synapse and biofilm-mediated transmission are consistent with the fact that cell-free HTLV-1 particles are usually undetectable in the serum of HTLV-1 infected subjects, and cell-free blood products are not infectious.

After virus entry into the target cell, the viral genome is reverse-transcribed by reverse transcriptase (RT), producing an RNA-DNA hybrid. Ribonuclease H (RNAse H) degrades the RNA strand, while the DNA strand is used as a template by RT to synthesize a complementary DNA strand; the double stranded DNA circularizes and transfers to the nucleus, where it integrates randomly in the host genome. Integration is mediated by the viral enzyme integrase and by the long terminal repeats (LTRs) located at the ends of the viral genome. Viral genes are then transcribed and translated by using the cellular machinery. Virion assembly occurs in the cytoplasm, through the interaction between the viral nucleocapsid and the plasma membrane, and incorporation of two copies of the RNA genome along with tRNA, RT, protease, and integrase.

1.3 HTLV-I genetic organization

The basic structure of the Deltaretrovirus genome consists of the LTRs at the 5’ and 3’ ends of the genome, and Gag, pro, pol and env genes that code for enzymes and structural proteins of mature virus particles. The region between the env gene and 3’ LTR is termed the X region, and contains at least five partially overlapping open readings frames (ORFs), termed x-I through x-V, coding for regulatory and accessory proteins (Figure 1). Expression of the highly condensed HTLV-1 genetic

information is achieved through ribosomal frameshifting (which generates a Gag-Pro-Pol polyprotein from the full-length transcript), and by alternative splicing (which produces distinct mRNAs coding for the env and X region genes). The HTLV-1 transcripts have been grouped in three major classes (Figure 2): a) unspliced (US) mRNA, coding for gag-pro-pol, and used as genomic RNA; b) singly-spliced (SS) mRNAs, coding for the envelope glycoproteins (Env) and for the accessory proteins $p21^{Rex}$, p12 and p13; c) doubly-spliced (DS) mRNAs, coding for the regulatory proteins $p40^{Tax}$ (Tax) and $p27^{Rex}$ (Rex), and for the regulatory/accessory protein p30.

The negative strand of HTLV-1 codes for the HBZ protein (HTLV-1 bZIP factor) (Gaudray et al., 2002). The ORF coding for HBZ is located in the X region (antisense orientation) and is transcribed from a promoter in 3' LTR (Larocca et al., 1989).

1.4 Expression of structural proteins

The full length US mRNA (8.2 kb) is packaged into virions as the genomic RNA and is also translated into the Gag, Protease and Polymerase proteins (Lairmore and Franchini, 2007). These genes are translated as a polyprotein precursor which is cleaved to form the mature gag peptides: 19 kDa matrix (MA), 24 kDa capsid (CA), and 15 kDa nucleocapsid (NC). The gag polyprotein is post-transcriptionally modified by myristylation at its N-terminus, an essential step for its insertion in the plasma membrane of the infected cell. A first ribosomal frameshifting event produces a Gag-Protease polyprotein precursor. The protease gene encodes the viral Protease, which is essential for the cleavage of the Gag precursor. The pol gene is also translated as a polyprotein precursor, with the 5’ portion encoding the RT protein, which converts the viral single-stranded RNA genome into double stranded DNA. Sequences downstream code for Integrase, which is responsible for the integration of the reverse-transcribed viral genome in the host cell genome, and for RNaseH, which degrades the viral RNA genome in the context of the DNA/RNA hybrid produced by the first strand synthesis step of the reverse transcription process.

The env gene partially overlaps with the 3’ end of pol (Figure 2). The 68 kDa Envelope precursor is modified by glycosylation and cleavage into two proteins named gp46-SU, localized in the surface of infected cells and virions and responsible

for the binding to the cell receptor GLUT-1, and gp21-TM, a transmembrane protein that mediates membrane fusion and formation of the virological synapse.

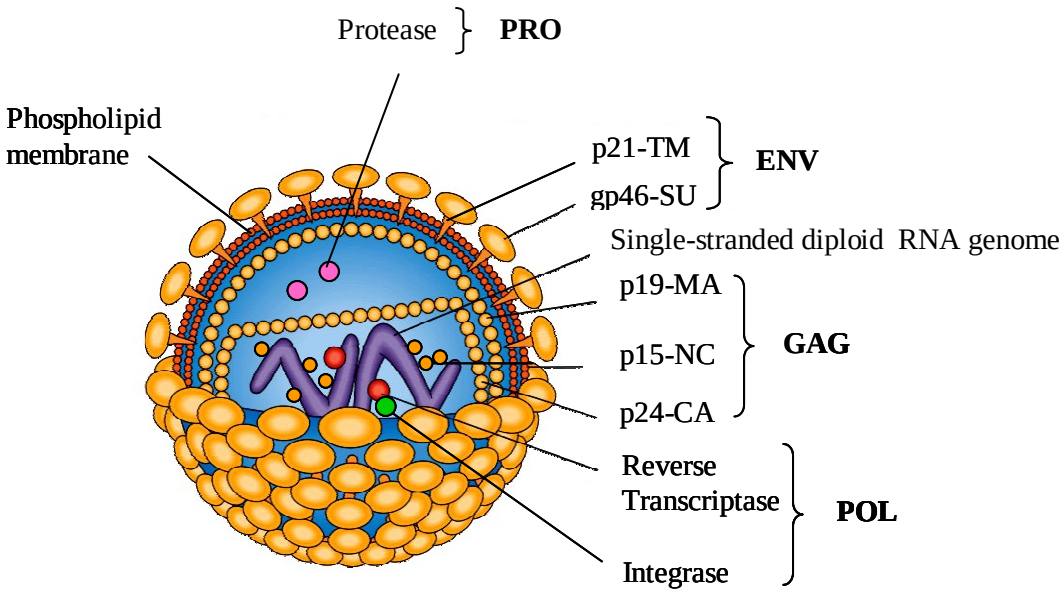

Figure 1: Schematic representation of the HTLV-1 virion (Le Blanc et al., 2001)

1.5 Expression of proteins coded in the X region

The X region of the HTLV-1 genome contains at least four different open reading frames that code for non structural accessory and regulatory proteins. As shown in Figure 2, expression of the different, partially overlapping ORFs of the X region is accessed through alternative splicing. All these mRNAs contain exon 1, which is non coding. Singly spliced mRNAs contain exon 1 and different 3' regions, and code for the envelope proteins and for the accessory proteins p13 (translated from ORF x-II, mRNA 1-C), p12 (translated from ORF x-I, mRNA 1-A or 1-B) (Ciminale et al., 1992; Koralnik et al., 1992), and $p21^{Rex}$ (translated from ORF x-III, mRNA 1-3). Two doubly spliced mRNAs contain exons 1 and 2, and different 3' regions: the former is a bicistronic transcript coding for the regulatory proteins Rex and Tax (translated from x-III and x-IV ORFs, respectively, exons 1, 2 and 3), the latter codes for the accessory/regulatory protein p30 (translated from x-II ORF, exons 1, 2 and B) (Ciminale et al., 1992; Koralnik et al., 1992).

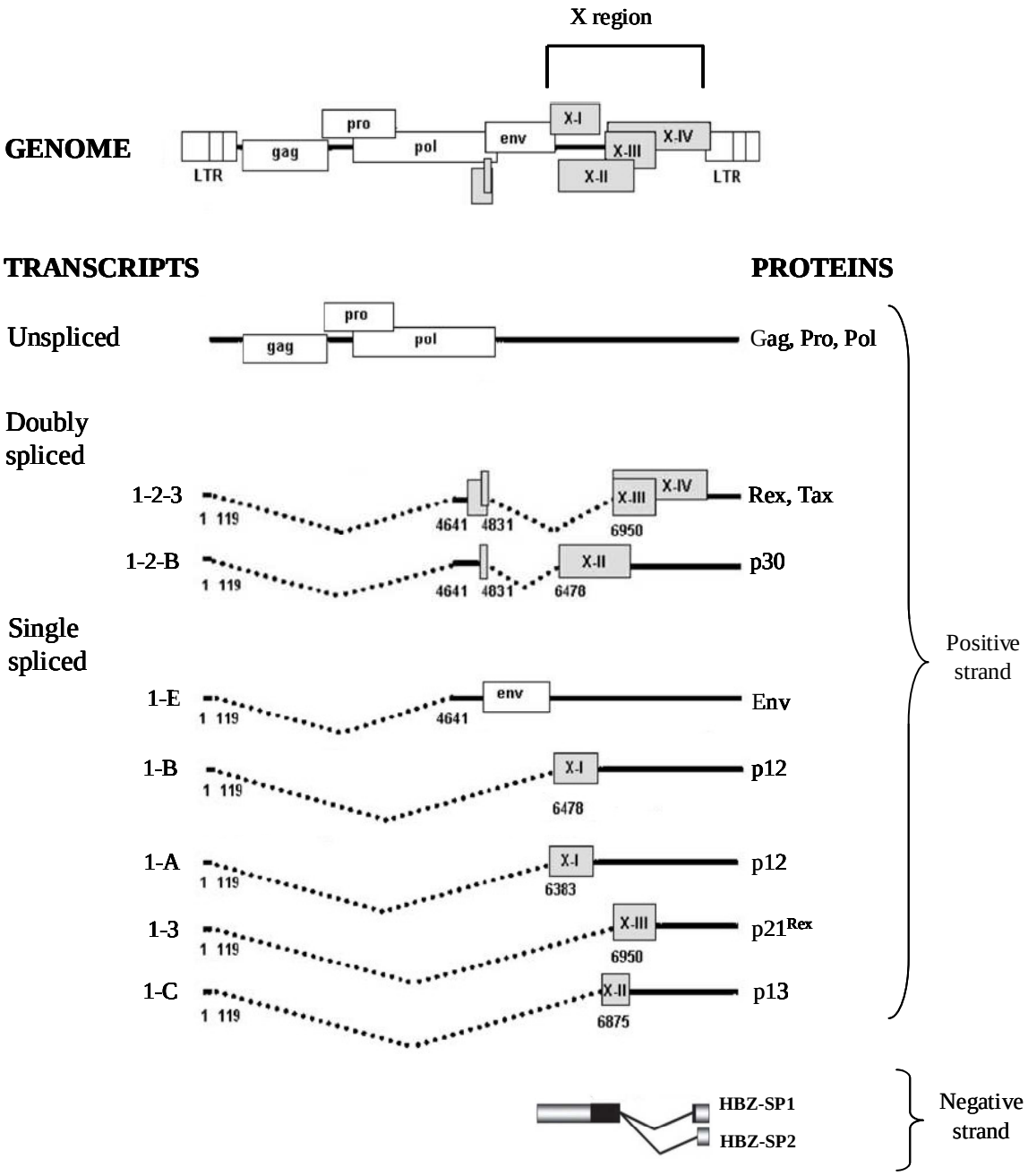

Figura 2. Organization and expression of the HTLV-1 genome. ORFs, transcriptional map of HTLV-1, and proteins coded by each mRNA are shown. The numbering indicates splicing sites used for the generation of the mature mRNAs. Resulting exons are: 1 (1-119), 2 (4641-4831), 3 (6950-9067), A (6383-9067), B (6478-9067), C (6875-9067) and E (4641-9067). mRNAs are named according to thier exonic composition (Nicot et al., 2005).

1.6 Function of the proteins encoded in the X region

1.6.1 Rex

Rex is a 189-amino acid, 27-kDa nuclear phosphoprotein that controls viral gene expression at the post-transcriptional level by binding to an RNA element termed the Rex-responsive element (RxRE), a highly stable stem-loop structure located in the 3' LTR (Younis and Green, 2005). The Rex-RxRE interaction promotes transport of US and SS viral mRNAs out of the nuclear compartment, a function that is tightly linked to Rex's ability to shuttle between the nucleus and the cytoplasm (Narayan et al., 2003).

Three main functional domains have been mapped in the Rex protein sequence: a) an N-terminal arginine-rich region important for nuclear localization and binding to the RxRE (Siomi et al., 1988); b) a leucine-rich sequence located near the middle of the protein that functions as a nuclear export signal (NES) and interacts with the nuclear export receptor, CRM-1/exportin1 (Bogerd et al., 1995; Hope et al., 1991); and c) regions flanking the NES that are required for the assembly of Rex into multimeric structures upon binding to the RxRE (Bogerd and Greene, 1993). CRM-1 belongs to the importin-β family, whose members act as RNA transporters between nuclear and cytoplasmic compartments by binding to nucleoporin hRIP/Rab and Nup214/CAN (Bogerd et al., 1998). In addition to acting as an RNA chaperone, Rex is able to inhibit splicing *in vitro,* during the initial phase of spliceosome formation (Bakker et al., 1996). Although Rex is not required for cellular immortalization *in vitro,* it is necessary for infectivity and viral persistence *in vivo* (Ye et al., 2003), since expression of the US and SS viral RNAs encoding structural proteins is necessary for the assembly of virions. The fact that these mRNAs depend on Rex for expression suggests that the Rex-RxRE interaction may function as a molecular switch controlling the transition between productive and latent phases of HTLV-1 infection. Rex function is modulated by phosphorylation on serine/threonine residues (Adachi et al., 1990; Kesic et al., 2009), a property that highlights the importance of cellular factors in the multi-level regulation of HTLV gene expression (Younis and Green, 2005).

1.6.2 Tax

Tax is a 352-amino acid, 40-kDa phosphoprotein that is essential for activation of transcription from the LTR promoter (Gatza et al., 2003). The following functional domains have been mapped in the Tax sequence: a hydrophobic N-terminal domain, a zinc finger, a leucine-rich region, and a C-terminal acidic alpha helix.

The N-terminal region contains sequences important for nuclear localization (nuclear localization signal, NLS). The zinc finger is important for interactions with cellular transcriptional factors and/or for Tax dimerization. The central leucine-rich sequence is similar to the leucine zipper found in the Fos/Jun family of transcriptional activators.

In addition to activating transcription from the viral LTR promoter through three 21-base pair repeat elements named TRE (Tax-responsive elements), Tax stimulates transcription of a large number of cellular genes. Transcriptional activation by Tax is mediated through interactions with cellular transcription factors including CREB-ATF family members, serum responsive factors (SRF) and NF-κB (Kashanchi and Brady, 2005). Tax interacts with the CREB transcription factors and with the CBP/p300 and pCAF co-activators, which control chromatin remodelling through the acetylation of core histones. The interaction of CREB and CBP/p300 is controlled by phosphorylation of CREB in response to different signal transduction pathways (e.g. PKA and CAMK). In contrast, in the presence of Tax, this pathway is constitutively activated through binding of Tax to CBP/p300. The end result of these interactions is constitutive activation of CREB-responsive genes by Tax.

The active form of NF-κB is a heterodimeric protein composed of two subunits of 50 kDa and 65 kDa. In the absence of mitogenic stimulation, the NF-κB complex is sequestered in the cytoplasm, where it is associated with the inhibitory subunit I-κB. Following cellular activation, I-κB is rapidly phosphorylated by IKKβ (I-κB kinase) and targeted for ubiquitination and proteasomal degradation. Following release from I-κB, NF-κB translocates to the nucleus, where it drives transcription of target genes. It has been shown that Tax increases IKKγ activity, thus enhancing I-κB degradation and NF-κB activation (Sun and Yamaoka, 2005).

Tax is recruited by SRF to specific cellular promoters of immediate-early genes such as c-Fos and early growth response genes 1 and 2. The engagement of the CBP/p300 coactivators is also required for transcriptional activation of the SRF pathway by Tax (Shuh and Derse, 2000).

In addition to these transcriptional effects, Tax interacts with $p16^{INK4A}$ and inhibits its suppression of CDK4. Tax also binds to cyclin D, resulting in increased CDK4 activity and phosphorylation of cyclin D. These interactions result in deregulation of the Rb pathway controlling entry into the S phase of the cell cycle and drive cell proliferation (Li et al., 2003).

Tax also interacts with the anaphase promoting complex (APC), which controls the metaphase-anaphase transition and correct execution of mitosis. APC directs the ubiquitination and proteosomal degradation of cyclin B1 and Pds1p/securin, key regulators of mitosis. Both securin and cyclin B act by inhibiting separase, a protease that destroys the connections linking sister chromatids. In normal cells chromosomes start to segregate only after they have been attached to the kinetocore and are subjected to mechanical tension (Nasmyth, 2005). In Tax-positive cells the decrease in cyclin B and securin starts in S phase, before the cell enters mitosis. This results in incorrect activation of separase and unequal chromosomal separation between cells (Liu et al., 2005).

Furthermore, Tax inactivates the p53 tumor suppressor, thus impinging on the major pathway controlling genome integrity and favouring the emergence of a large spectrum of molecular alterations in infected cells (Tabakin-Fix et al., 2005).

Experimental evidence accumulated so far underscores the role of Tax as an essential effector of HTLV-1 mediated tumorigenicity. Tax expression induces an immune response since it is the major target of cytotoxic T lymphocytes (CTLs). To escape from CTLs, ATLL cells frequently lose the expression of Tax by several mechanisms (loss of the viral promoter, nonsense or missense mutation of the tax gene, epigenetic change by hypermethylation). Thus, it is speculated that Tax plays an important role in the persistent proliferation of HTLV-1-infected cells during the carrier state, with the mutator phenotype conferred by Tax promoting accumulation of genetic and epigenetic changes in the host genome that finally lead to Tax-independent proliferation and escape from the host immune system by inactivation of Tax (Yasunaga and Matsuoka, 2007).

1.6.3 HBZ

HBZ is a 31-kDa protein coded by the minus strand of the viral genome. The HBZ ORF and start codon are located within the X region. HBZ localizes in the nucleus through three NLSs (Hivin et al., 2005), and contains an N-terminal transcriptional activation domain and a leucine zipper in the C-terminal portion (Gaudray et al., 2002). HBZ is not necessary for viral replication and immortalization *in vitro*, but increases infectivity and viral persistence *in vivo* (Arnold et al., 2006).

HBZ interacts with a number of transcription factors, including CREB, p300/CBP, Jun family members, and NF-κB (Matsuoka and Green, 2009). HBZ directly interacts with CREB and p300/CBP, suppressing Tax-induced viral transcription (Gaudray et al., 2002; Lemasson et al., 2007), thus acting as negative modulator of Tax. Binding to JunB and to c-Jun by HBZ causes the suppression of their transcriptional activity, by sequestration into nuclear bodies (JunB) or by blocking DNA binding activity (c-Jun), and by promoting their proteasomal degradation (Basbous et al., 2003; Matsumoto et al., 2005). Binding of HBZ to JunB and c-Jun prevents their interaction with Fos, repressing both viral and cellular AP-1 transcription. The interaction of HBZ with Jun-D stimulates its transcriptional activity (Thebault et al., 2004), and results in the activation of JunD-dependent cellular genes including human telomerase (hTERT) (Kuhlmann et al., 2007). HBZ has been shown to bind the NF-κB subunit p65 and inhibit the activation of the classical NF-κB pathway (Zhao et al., 2009).

Expression of HBZ mRNA leads to upregulation of E2F1 target genes and stimulates T-cell proliferation (Arnold et al., 2008; Satou et al., 2006). The fact that the 3' LTR region is neither deleted nor methylated (unlike the 5' LTR) in ATLL cells suggests that HBZ expression in primary cells obtained from ATLL patients plays a critical role in the development of this disease.

1.6.4 $p21^{Rex}$

$p21^{Rex}$, coded by the X-III ORF, is a truncated isoform of Rex lacking the N-terminal arginine-rich domain of the full-length protein. It acts as a repressor of full-length Rex, thereby inhibiting the expression of transcripts coding for structural proteins, enzymes and accessory proteins (Heger et al., 1999). It was thus hypothesized that $p21^{Rex}$ might play a role as a latency-inducing factor in the HTLV-1 life cycle.

1.6.5 p12

p12 is coded by the x-I ORF and is expressed from an singly-spliced mRNA (mRNA 1-A). p12 localizes in the endoplasmic reticulum (ER) and in the Golgi apparatus (Ding et al., 2001; Johnson et al., 2001; Koralnik et al., 1993). While this protein is not required for HTLV-1 replication *in vitro*, it plays a key role in the stabilization of a productive viral infection *in vivo* (Albrecht et al., 2000; Collins et al., 1996; Derse et al., 1997; Robek et al., 1998).

p12 is a higly hydrophobic protein, whose amino acidic sequence contains four proline-rich Src homology 3 (SH3) domains that mediate interactions with proteins involved in cell signal transduction, two trans-membrane leucine zipper motifs that mediate targeting of the protein to the ER and other endomembrane compartments (Ding et al., 2001; Johnson et al., 2001; Koralnik et al., 1993), and a calcineurin-binding motif (Kim et al., 2003).

p12 interacts with the β and γ_c chains of the IL-2R, resulting in their reduced surface expression (Mulloy et al., 1996). Furthermore, p12 binds to the cytoplasmic domain of the IL-2R β chain, which is involved in the recruitment of the Janus-associated kinases 1 and 3 (Jak1 and Jak3). This interaction determines an increase in the transcriptional activity of the signal transducers and activators of transcription-5 (STAT-5), providing a proliferative advantage to T cells (Nicot et al., 2001).

p12 was also shown to sequester free MHC class I heavy chains (MHC-I-Hc), preventing their binding to β2-microglobulin. p12-bound MHC-I molecules are translocated in the cytosol where they are degraded by the proteasome. The overall result of this interaction is a decrease in functional MHC-I on the surface of HTLV-1 infected cells that would thus escape from CTL recognition and clearance by the immune system (Johnson et al., 2001). Furthermore, p12 causes a reduction in the expression of ICAM-1 and ICAM-2, which mediate adhesion of natural killer (NK) cells to the infected cells, resulting in the protection of HTLV-1-infected primary CD4+ T cells from NK cell-mediated cytotoxicity (Banerjee et al., 2007)**.** This effect is particularly relevant in the context of HTLV-1 infection, which is able to induce a strong humoral and cellular immunitary response (Bangham, 2003).

Furthermore, p12 interacts with calreticulin and calnexin (Ding et al., 2001), two ER-resident proteins that regulate Ca^{2+} storage and release, and reduces the amount of Ca^{2+} released from the store while increasing cytosolic Ca^{2+} level, suggesting a p12-mediated Ca^{2+} leakage from the ER (Ding et al., 2002). Moreover, p12 induces

nuclear factor of activated T-cells (NFAT) activation (Albrecht et al., 2002), by interacting with calcineurin, a Ca^{2+}-responsive protein phosphatase that controls NFAT activity (Kim et al., 2003). Taken together these effects decrease the threshold for T-cell activation and proliferation (Nicot et al., 2005).

The modulation of Ca^{2+} homeostasis and signalling induced by p12 are in line with a recent study demonstrating that HTLV-1 infected cells possess alterations in Ca^{2+} homeostasis and gene expression (Akl et al., 2007). Furthermore, the modulation of Ca^{2+} signalling is a shared mechanism for different viruses to facilitate their infection (Chami et al., 2006; Zhou et al., 2009): HIV-1 Nef and HCV core are some examples of virally encoded proteins controlling Ca^{2+} levels, Ca^{2+}-dependent transcription, and infectivity (Bergqvist et al., 2003; Manninen and Saksela, 2002).

1.6.6 p30

The x-II ORF is translated from two alternatively spliced mRNAs (1-2-B and 1-C) into two proteins, termed p30 and p13 (D'Agostino et al., 2001). An HTLV-1 molecular clone containing a mutation in the x-II ORF affecting p30 and p13 expression is still able to produce infective virions and immortalize human T-lymphocytes (Robek et al., 1998), but shows a drastic reduction in *in vivo* infectivity in animal models (Bartoe et al., 2000).

p30 is a 241-amino acid nucleolar-nuclear protein (Ciminale et al., 1992) that contains a bipartite arginine-rich NLS (D'Agostino et al., 1997). p30 functions at the post-transcriptional level by inhibiting the nuclear export of the tax-rex mRNA; this effect results in a global inhibition of viral gene expression, suggesting that p30 might function as a latency-inducing factor (Nicot et al., 2004; Younis et al., 2004). Unlike Rex, p30 does not contain a recognizable NES, and does not appear to shuttle from the nucleus to the cytoplasm (D'Agostino et al., 1997), properties consistent with its role as a nuclear-retention factor for RNA. p30 interacts with Rex, and this interaction is enhanced in the presence of viral RNA, suggesting that p30 may function by binding Rex in complex with viral RNA, thereby inhibiting Rex-dependent RNA export (Sinha-Datta et al., 2007).

In addition to regulating the export of the tax/rex mRNA to the cytoplasm, p30 expression modifies a number of signalling pathways such as TLR4, CREB, and GSK3β (Datta et al., 2006; Zhang et al., 2001; Zhang et al., 2000). Studies aimed at analyzing the regulation of gene expression by p30 demonstrated that genes involved

in transcriptional/translational control, cell cycle, DNA replication and repair, apoptosis, and cell signalling are affected by p30 (Awasthi et al., 2005; Michael et al., 2004; Taylor et al., 2009), suggesting that some of these genes might play a role in cell transformation.

p30 thus possesses both transcriptional and post-transcriptional activities. The combination of these effects likely decreases expression of Tax and other viral antigens, possibly permitting HTLV-1 infected cells to remain hidden from the immune response (Taylor et al., 2009).

1.6.7 p13

p13 is a 87-amino acid protein that corresponds to the C-terminal portion of p30 (Koralnik et al., 1992) and accumulates in mitochondria (Ciminale et al., 1999). *In vivo* studies suggested that p13 is required for persistent infection in a rabbit model (Hiraragi et al., 2006).

Immunoelectron microscopy and fractionation experiments demonstrated that p13 is an integral membrane protein and accumulates mainly in the inner mitochondrial membrane (D'Agostino et al., 2005b; D'Agostino et al., 2000), although it is occasionally detected in the nucleus (D'Agostino et al., 1997; Koralnik et al., 1993). p13 induces specific alterations in mitochondrial morphology, resulting in isolated clusters of round-shaped, apparently swollen mitochondria, some of which form ring-like structures (Ciminale et al., 1999; D'Agostino et al., 2005b) (Figure 3A).

Functional mapping studies demonstrated that p13 contains a mitochondrial targeting signal (MTS) spanning amino acids 21-30 (Ciminale et al., 1999) that contains 4 arginines in the positions 22, 25, 29 and 30 (Figure 3B). The MTS of p13 (LRVWRLCTRR) is predicted to form an α-helix, with the 4 arginines forming a positively charged face that imparts amphipathic properties to this region (D'Agostino et al., 2002) (Figure 3C). Biophysical and biochemical analyses of a synthetic peptide spanning residues 9-41 ($p13_{[9-41]}$) confirmed that this region folds into an amphipathic α-helix upon exposure to membrane-mimetic solutions (D'Agostino et al., 2002). Although p13 mutants carrying substitutions of the arginines with glutamines, prolines, or alanines and leucines retain mitochondrial targeting, they produce little or no mitochondrial fragmentation/swelling, indicating that the arginines of the amphipathic α-helical domain are essential for these effects

(D'Agostino et al., 2002). In contrast to canonic MTSs, the targeting signal of p13 is not cleaved upon import into mitochondria (Ciminale et al., 1999).

In vitro assays carried out using isolated rat liver mitochondria and purified synthetic p13 demonstrated that the peptide changed K^+ permeability of isolated mitochondria. The K^+ influx into the mitochondrial matrix induced by p13 required the presence of the critical arginine residues, was dose-dependent, was driven by the mitochondrial membrane potential ($\Delta\psi$), and was accompanied by swelling (D'Agostino et al., 2002; Silic-Benussi et al., 2009). Increased K^+ permeability was associated with a dose-dependent reduction in $\Delta\psi$. p13 also induced an increase in respiratory chain activity, oxygen consumption and in the production of reactive oxygen species (ROS), and reduced the threshold for permeability transition pore (PTP) opening (Silic-Benussi et al., 2009).

Cells expressing p13 exhibit reduced proliferation rates and increased sensitivity to apoptosis triggered by Fas L and ceramide (Hiraragi et al., 2005; Silic-Benussi et al., 2004). It was observed that cells stably expressing p13 showed a marked increase in the Ca^{2+}-mediated phosphorylation of the transcription factor CREB (Silic-Benussi et al., 2004), suggesting that p13 might alter Ca^{2+} homeostasis and signalling.

p13 also interferes with the ability of HeLa cells and Ras/Myc-transformed primary fibroblasts to grow as tumors in nude mice, suggesting that it may exert tumor-suppressor-like activity (Silic-Benussi et al., 2004).

Analysis of living cells expressing p13-GFP and incubated with TMR, a $\Delta\psi$-dependent probe, indicated that the protein depolarizes mitochondria in some cells, while others maintain $\Delta\psi$ (Ciminale et al., 1999). This findings suggests that the effects of p13 in living cells might be subjected to regulation. Post-translational modifications, or pathophysiological changes affecting mitochondrial functions (e.g. the activity of the respiratory chain, the availability of substrates, or stress conditions) might affect p13 function. Several viral proteins are regulated by post-translational modifications mediated by cellular kinases/phosphates. An example is influenza A virus (IAV) PB1-F2 which localizes to mitochondria, has proapoptotic activity, and shares structural and functional similarities with p13 (Gibbs et al., 2003). Recent studies demonstrated that PB1-F2 is phosphorylated by protein kinase C (PKC) at several sites, with functional mutation of these sites resulting in reduced cell death and reduced virus titres in infected monocytes (Mitzner et al., 2009).

In the context of HTLV-1 infection, both Tax and Rex are known to be regulated through phosphorylation, resulting in the regulation of CREB and NF-κB transactivating function (Durkin et al., 2006), and of structural protein expression (Adachi et al., 1990; Kesic et al., 2009).

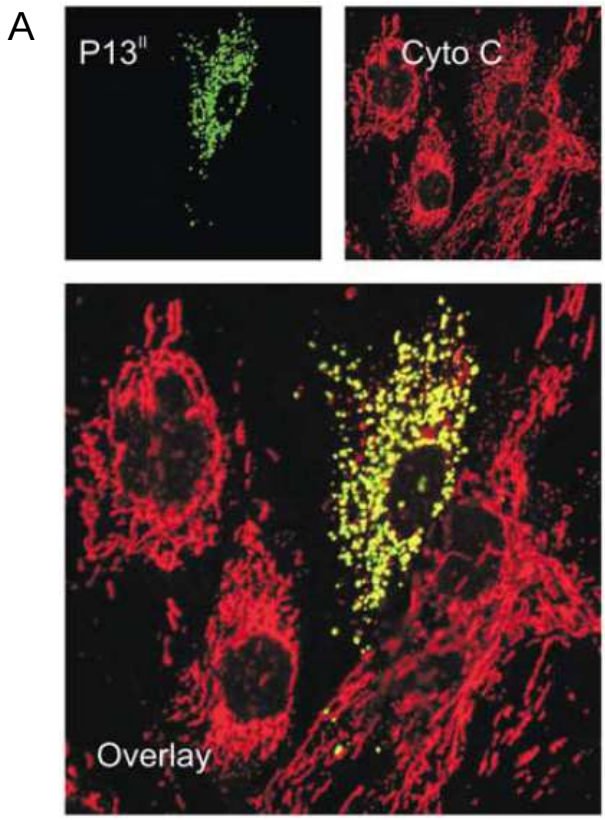

B
MLIISPLPRV WTESSFRIPS (1-20)
LRVWRLCARR LVPHLWGTMF (21-40)
GPPTSSRPTG HLSRASDHLG (41-60)
PHRWTRYQLS STVPYPSTPL (61-80)
LPHPENL (81-87)

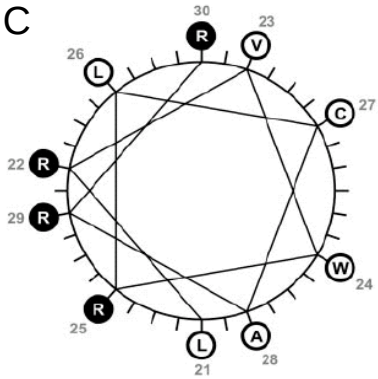

Figure 3. The amino acid sequence and mitochondrial targeting of p13. Panel A shows the subcellular targeting of p13 and its effects on mitochondrial morphology. Shown is an indirect immunofluorescence assay of p13-transfected HeLa cells; p13 is detected as a green signal and the mitochondrial marker protein cytochrome c as a red signal; in the cell expressing p13, the two signals overlap, producing a yellow signal. The cell expressing p13 contains mitochondria with marked alterations in morphology suggestive of fragmentation and swelling. B shows the amino acid sequence of p13 coded by molecular clone CS-HTLV-1. The 10-residue MTS shown in a previous study to be sufficient for targeting of green fluorescent protein to mitochondria (residues 21–30) is underlined. C shows a helical wheel model of the p13 MTS, illustrating partitioning of hydrophobic and positively charged residues on opposite sides of the helix. C

1.7 Basic functions of mitochondria

Mitochondria are complex organelles bound by two highly specialized membranes that define four mitochondrial sub-compartments: outer membrane, inter-membrane space, inner membrane, and matrix. Mitochondria play a key role in energy production and aerobic metabolism as they are the site of oxidative phosphorylation, the Krebs cycle and β-oxidation of fatty acids. Furthermore, mitochondria contribute to the control of apoptosis and modulate the duration and amplitude of cytosolic Ca^{2+} transients, thus influencing the major Ca^{2+}-dependent signal transduction pathways. In addition, the mitochondrial respiratory chain is the major site of reactive oxygen species (ROS) production within the cell. ROS have recently emerged as important mediators of both cell activation and death (Rustin, 2002).

Mitochondria exhibit an ordered compartmentalization of the enzymatic complexes mediating the different mitochondrial functions. The inner mitochondrial membrane (IMM) forms numerous invaginations, termed cristae, that increase its total surface. The IMM contains proteins with three different functions: a) complexes of the respiratory chain; b) the ATPase enzymatic complex F_0F_1 that synthesizes ATP starting from ADP and phosphate; and c) specific transport proteins that regulate the passage of ions and metabolites. The matrix contains the Krebs cycle and β-oxidation enzymes and the mitochondrial genome with its transcriptional and translational apparatus.

Oxidative phosphorylation consists of the transfer of electrons from NADH to molecular oxygen to generate water. This process, which is broken up into several intermediate steps driven by the complexes of the respiratory chain, is coupled with the extrusion of protons through the IMM, thus generating an electrochemical gradient that can be utilized by the ATPase as a driving force for the synthesis of ATP.

Proteins of the Bcl-2 family and the PTP are responsible for the mitochondrial membranes permeabilization, the release into the cytosol of the apoptogenic factors confined in the intermembrane space, and the consequent induction of apoptosis (Kroemer et al., 2007; Rasola and Bernardi, 2007). Upon release from mitochondria, cytochrome c interacts with the adapter protein apoptosis protease activating factor-1 (APAF-1), which in turn activates the caspase protein family, resulting in the execution of apoptosis. Mitochondria release apoptosis inducing factor (AIF) and

endonuclease G (Endo G), which translocate to the nucleus and activate the fragmentation and condensation of genomic DNA, a distinctive feature of the late stages of apoptosis. Other released proteins include Smac/DIABLO and Omi/HtrA2, which antagonize IAP proteins, deputated to prevent procaspases activation.

1.8 Mitochondria and calcium homeostasis

The amplitude, frequency and duration in cytosolic Ca^{2+} transients constitute a complex signalling pathway that controls a vast number of biological responses ranging from muscle contraction to secretion, control of transcription, and apoptosis. The increase in Ca^{2+} cytosolic concentration is determined by Ca^{2+} mobilization from intracellular stores (mainly the ER and Golgi apparatus), through the activation of IP3 (inositol 1,4,5-trisphosphate) or ryanodine receptors, and the entry from the extracellular milieu through plasma membrane Ca^{2+} channels (Store-operated Ca^{2+} channels, SOCs; Voltage-operated Ca^{2+} channels, VOCs; Receptor-operated Ca^{2+} channels, ROCs; Second Messenger-operated Ca^{2+} channels, SMOCs). The Ca^{2+} signal is rapidly terminated by Ca^{2+} extrusion, mediated by the activity of the Plasma Membrane Ca^{2+}-ATPase (PMCA) and of the Na^{+}/Ca^{2+} exchanger (NCX), localized in the plasma membrane, and by the refilling of the intracellular store. Mitochondria also play a key role in the Ca^{2+} homeostasis. Mitochondrial Ca^{2+} uptake is driven by the mitochondrial inner membrane potential ($\Delta\psi$), generated by the activity of the electron transport chain, and is mediated by the Ca^{2+} uniporter, localized in the inner membrane (Kirichok et al., 2004), and by rapid uptake mode (RaM) (Gunter et al., 2004). Mitochondrial efflux requires Na^{+}/Ca^{2+} and H^{+}/Ca^{2+} exchangers or Permeability Transition Pore (PTP) opening (Rasola and Bernardi, 2007). Mitochondrial Ca^{2+} uptake occurs mainly in restricted spatial domains in proximity to the ER (mitochondria-ER microdomains) or with the plasma membrane, resulting in spatio-temporal confinement of cytosolic Ca^{2+} spikes and in the modulation of plasma membrane Ca^{2+}-dependent channels. An increase in Ca^{2+} concentration in the mitochondrial matrix upregulates the activity of Ca^{2+}-sensitive dehydrogenases, involved in ATP production and oxidative metabolism. Furthermore, mitochondrial fusion and fission are Ca^{2+}-dependent processes (Cereghetti and Scorrano, 2006; Rizzuto et al., 2003; Szabadkai et al., 2006). On the other hand, excessive accumulation of mitochondrial Ca^{2+} causes PTP opening, matrix swelling, and release of apoptogenic factors, leading to caspase activation and cell death.

The increase in intracellular Ca^{2+} plays a key role in controlling T-cell activation and proliferation. The major pathway involved is through store-operated Ca^{2+} entry (SOCE), mediated by Ca^{2+}-release-activated Ca^{2+} (CRAC) channels (Lewis, 2007). CRAC channels, localized in the plasma membrane, are activated by Ca^{2+} store depletion following TCR engagement, IP3 production and Ca^{2+} release from the ER (Feske, 2007). Recent studies demonstrated that functional and polarized mitochondria enhance CRAC activity and Ca^{2+} signal amplitude. Translocation of mitochondria to the immunological synapse is essential for T cell activation (Hoth et al., 2000; Quintana et al., 2006; Quintana et al., 2007).

1.9 Tumor viruses, mitochondria, and Ca^{2+}

Recent studies demostrated that several viruses code for mitochondria-targeted proteins, which, although by different mechanisms, have relevant effects on mitochondrial functions, and consequently on cell turnover, apoptosis, and neoplastic transformation (Boya et al., 2004; D'Agostino et al., 2005b). Furthermore, modulation of Ca^{2+} signalling pathways is a common mechanism employed by viruses to maximize dissemination and persistence of infection. Viral proteins may impinge on Ca^{2+} homeostasis through direct binding to Ca^{2+}, modification of membrane permeability, or alteration of the activity of individual signalling components (e.g., channels, pumps, chaperones, calcium sensors, transcription factors) (Chami et al., 2006; Zhou et al., 2009)

One example of a viral protein affecting the mitochondria-Ca^{2+} signal connection is HBV HBx protein, which colocalizes with the voltage-dependent anionic channel-3 (VDAC3), a component of the PTP, induces a perinuclear mitochondrial distribution coupled to fragmentation, swelling, $\Delta\psi$ loss, a reduction in mitochondrial Ca^{2+} uptake, and apoptosis (Chami et al., 2003; Rahmani et al., 2000; Shirakata and Koike, 2003; Takada et al., 1999). Overexpression of HBx enhances agonist-evoked cytosolic Ca^{2+} signals, due to decreased PMCA activity, resulting from its cleavage mediated by caspase 3, whose activity is increased in HBx-expressing cells (Chami et al., 2003). Vpr, encoded by HIV-1, also localizes in mitochondria, where it promotes apoptosis through mitochondrial membrane permeabilization and cytochrome c release. The C-terminal domain of Vpr folds into an α-helix that contains three arginines essential for the protein's interaction with the adenine nucleotide translocase (ANT) (Jacotot et al., 2000).

Some virus-encoded proteins are classified as viroporins, which are small viral proteins that contain transmembrane amphipathic α-helical domains whose multimerization in the context of membranes results in the formation of channel-like structures (Gonzalez and Carrasco, 2003). p13's ability to increase mitochondrial K^+ permeability and in turn influence mitochondrial $\Delta\psi$ depends on the integrity of its amphipathic α-helix. This property, together with its propensity to form high-molecular weight complexes (D'Agostino et al., 2002) suggests that p13 may function as a viroporin. One interesting example of a viroporin is p7 of hepatitis C virus (HCV), a 63–amino acid protein that accumulates primarily in the ER (Haqshenas et al., 2007). p7 is necessary for both entry and release of viral particles (Steinmann et al., 2007) and is required for HCV infection in the chimpanzee model (Sakai et al., 2003). The functional properties of p7 are attributed to its ability to form a hexameric cation channel that shows selectivity for Ca^{2+} over K^+ (Griffin et al., 2003) and whose activity is inhibited by amantadine and long alkyl chain iminosugar derivatives (Griffin et al., 2003; Pavlovic et al., 2003). HIV-1 Vpu and influenza virus M2 are other examples of viroporins.

Interference with mitochondrial functions (D'Agostino et al., 2005a) and Ca^{2+} homeostasis (Zhou et al., 2009) are emerging as key components in the mechanism by which viral infection can favour cell transformation. Further investigation of p13's interactions with mitochondria and the Ca^{2+} signalsome, as well as its functional regulation by post-translational modifications, are therefore likely to provide important insights into the mechanisms of viral replication and tumorigenesis induced by HTLV-1 infection.

2. AIMS

Adult T-cell leukemia/lymphoma (ATLL) is a powerful model to gain insight into the mechanisms of T-cell leukaemogenesis, as development of ATLL is modulated by an interplay between cellular factors and HTLV-1 gene products. Our recent studies showed that p13, an 87-amino acid protein of HTLV-1, is targeted to the inner membrane of mitochondria and induces major changes of mitochondrial permeability and morphology, and affects T-cell turnover and tumor formation. The work described in the present thesis was focused on the following aspects of p13 function:

- the effect of p13 on mitochondrial membrane potential in living cells
- the effect of p13 on Ca^{2+} homeostasis
- the possible functional regulation of p13 by phosphorylation.

3. MATERIALS AND METHODS

3.1 Cell cultures

HeLa and the HeLa-derived cell line HeLa-Tat [used for its high transfection efficiency (Schwartz et al., 1990)], were maintained in DMEM (Sigma) supplemented with 10% fetal calf serum (FCS; Invitrogen), 100 units/ml penicillin, and 20 units/ml streptomycin. Jurkat T-cells were maintained in RPMI 1640 (Sigma) supplemented with 10% FCS, penicillin/streptomycin and 2 mM L-glutamine (GIBCO).

3.2 Plasmids

Plasmid pSGp13, expressing p13 under the control of the SV40 promoter, and derivatives in which arginines at positions 22, 25, 29, and 30 were mutated either to glutamines (pSGp13RQ), alanine-leucine-leucine-alanine (pSGp13RAL), or prolines (pSGp13RP), were previously described (D'Agostino et al., 2002). pSGp13S15A and pSGp13S15D, containing alanine and aspartic acid instead of serine in position 15, were generated by PCR-based plasmid mutagenesis (Quikchange, Stratagene) using pSGp13 as a template.

pcDNAp13-GFP, expressing p13 fused to enhanced green fluorescent protein, was constructed by inserting the fused gene into the CMV promoter-driven vector pcDNA3.1 (Invitrogen). pcDNAp13RQ-GFP (containing glutamines instead of arginines as described for pSGp13), pcDNAp13S15A-GFP and pcDNAp13S15D-GFP (mutated on serine 15 as described for pSGp13) were generated as described above. For brevity, these constructs and the encoded proteins were indicated as "p13-GFP", "p13RQ-GFP", "p13S15A-GFP", "p13S15D-GFP". Mutations were verified by DNA sequencing (Big Dye Kit, Applied Biosystems).

Plasmids expressing chimeric aequorins targeted to mitochondria (mtAEQmut), the cytosol (cytAEQ), and the endoplasmic reticulum (erAEQmut) were previously described (Pinton et al., 2007); "AEQ" refers to wild-type aequorin, and "AEQmut" refers to a low-affinity D119A mutant of aequorin. For a map of the constructs and detailed information on their characteristics, see (Chiesa et al., 2001).

Plasmid Lcxl expresses Tax under the control of the viral LTR (long terminal repat) promoter (Felber et al., 1985). This plasmid was used to increase the expression of p13 from the pSG plamids, when cotransfected in Jurkat T-cells.

3.3 Analysis of mitochondrial membrane potential in HeLa cells

HeLa-Tat cells were seeded at a density of 75,000 cells/ml onto 35 mm plates, cultured for 24 hours, and then transfected with a plasmid expressing either wild type p13 (p13WT-GFP) or mutants p13RQ-GFP, p13S15A-GFP, p13S15D-GFP using Fugene 6 reagent (Roche). Eighteen hours after transfection, the cells were incubated with tetramethyl rhodamine methyl ester (TMRM, Molecular Probes) for 30 minutes at 37°C in the presence of 20 μg/ml verapamil (Sigma) to block activity of the multidrug resistance pump and allow efficient and uniform TMRM loading (Dietel et al., 1994; Petronilli et al., 1998).

Cultures were transferred to a 37°C, 5%-CO2 incubator attached to a Zeiss LSM510 laser scanning microscope. Images of the living cells were obtained using a Helium Neon (543 nm) laser to excite TMRM and an Argon laser (488 nm) to excite GFP; laser intensity, pinhole aperture and photomultiplier parameters were standardized to allow comparable measurements. The mean fluorescence intensities of GFP and of TMRM in individual cells were quantitated using the the Zeiss "Histogram" software tool. At least 100 cells from four different randomly selected fields were measured for each experimental group comparing p13WT-GFP to p13RQ-GFP, while approximately 60 cells from three different randomly selected fields were considered for each experimental group comparing p13WT-GFP to the serine mutants (p13S15A-GFP and p13S15D-GFP). Expression levels of GFP-fusion proteins from at least three independent experiments were normalized to the respective mean value of fluorescence intensity of p13WT-GFP, while the $\Delta\psi$ values were normalized to the respective mean value of TMRM fluorescence intensity in control non-transfected cells. The normalized GFP fluorescence intensity values were used to separate cells into five groups with different levels of p13 expression; mean TMRM fluorescence values in these expression groups were plotted. Statistical analysis was carried out using Student's T test.

3.4 Analysis of mitochondrial membrane potential in Jurkat T-cells

Jurkat T-cells, maintained at the optimal growth density of 250,000 cells/ml, were transfected by electroporation (MicroPorator, Digital Bio). Briefly, 5×10^6 cells were washed in PBS and resuspended in 120 μl of buffer R (Digital Bio) containing 5 μg of plasmid expressing p13WT-GFP or p13RQ-GFP, and subjected to a single 30 msec pulse of 1,410 Volts. Cells were maintained at the density of 5×10^6 cells/ml in

RPMI with 10% FCS, 2 mM glutamine for 1 hour and then diluted to 1 x 10^6 cells/ml in complete RPMI. Twenty-four hours after electroporation, the cells were centrifugated and resuspended in complete RPMI supplemented with 10 mM HEPES, at final density of 500,000 cells/ml. Cells were then incubated with TMRM (Molecular Probes) for 30 minutes at 37°C in the presence of 20 μg/ml verapamil (Sigma). Samples were analyzed for GFP and TMRM fluorescence by flow cytometry using a FACSCalibur apparatus (Becton Dickinson Coulter) and CellQuest software (Becton Dickinson Biosciences), with 20,000 ungated events examined for each sample. Control samples transfected with Bluescript vector (BS), or not subjected to the incubation with TMRM and verapamil, were also analyzed. The percentage of cells with $\Delta\psi$ within the range of $\Delta\psi$ measured in control cells (transfected with BS) was analyzed after separating cells into subgroups of different expression levels of GFP-fusion proteins. Experiments were repeated three times and statistical analysis was carried out using Student's T test.

3.5 Analysis of Ca^{2+} homeostasis in HeLa cells

HeLa cells, maintained in complete DMEM, were seeded onto 13-mm glass coverslips, grown to 50% confluence, and transfected by calcium phosphate coprecipitation. Transfection mixtures contained 3 μg of a pSGp13 plasmid expressing wild-type p13 or the mutants in the four arginines (p13RQ, p13RP, p13RAL) or a control plasmid expressing mitochondrial-targeted GFP (mtGFP) (Rizzuto et al., 1995) and 1 μg of a plasmid expressing mtAEQmut, cytAEQ, or erAEQmut. For cytosolic and mitochondrial Ca^{2+} measurements, transfected HeLa cells were incubated with 5 μM coelenterazine for 1.5 hours in DMEM supplemented with 1% FCS and then transferred to the luminometer perfusion chamber. To efficiently reconstitute erAEQmut the luminal [Ca^{2+}] of the ER was reduced by incubating cells for 1 hour at 4 °C in modified Krebs-Ringer Buffer (KRB, containing 125 mM NaCl, 5 mM KCl, 1 mM $MgSO_4$, 1 mM Na_2HPO_4, 5,5 mM glucose and 20 mM HEPES) supplemented with 5 μM coelenterazine, 5 μM ionomycin (Sigma), and 600 μM EGTA. Cells were then extensively washed with KRB supplemented with 2% bovine serum albumin and 1 mM EGTA and transferred to the luminometer perfusion chamber. All aequorin measurements were performed in KRB supplemented with 1 mM $CaCl_2$. Histamine (100 μM) was used as an agonist. To discharge the residual aequorin pool and calibrate the signal, cells were

lysed with 100 μM digitonin in a hypotonic Ca^{2+}-rich solution (10 mM $CaCl_2$ in H_2O). The aequorin luminescence data were converted to [Ca^{2+}] values using a computer algorithm based on the Ca^{2+} response curve of wild-type and mutant aequorins as described previously (Pinton et al., 2007). Results were expressed as means ± standard error and analyzed for statistical significance using the Student's T test.

3.6 *In silico* analysis of p13's amino acidic sequence

The prediction of the possible kinases phosphorylating p13 was performed using the PROSITE database (Bairoch et al., 1997) and NetPhosK 1.0 algorithm (Blom et al., 1999). The prediction of the pI of the protein was performed by using Scansite prediction software (Obenauer et al., 2003).

3.7 Synthesis of $p13_{[9-22]}$ peptides (WT and S15A) and of full length $p13_{[1-87]}$ protein

p13-derived peptides ($p13WT_{[9-22]}$ and $p13S15A_{[9-22]}$) and full length p13 ($p13_{[1-87]}$) were synthesized by solid phase methods, in the laboratory of Prof. O. Marin (University of Padova, Department of Biological Chemistry), as described previously (D'Agostino et al., 2002; Silic-Benussi et al., 2009).

Briefly, peptides were synthesized with an Applied Biosystems Model 433 automated peptide synthesizer using the fluoren-9-ylmethoxycarbonyl (Fmoc) chemistry (Fields and Noble, 1990) and 2-(1H-benzotriazol-1-yl)-1,1,3,3-tetramethyluronium hexafluorophosphate (HBTU)/1-hydroxybenzotriazole (HOBt) or 2-(1H-7-azabenzotriazol-1-yl)-1,1,3,3-tetramethyl uronium hexafluorophosphate methanaminium (HATU) as coupling reagents and support resins specified below. Acetylation steps were carried out after every coupling of hydrophobic residues.

Peptides corresponding to amino acids 9-22 (RVWTESSFRIPSLR) of p13 were synthesized on Rink-Amide resin (Novabiochem) and cleaved from the solid support by 2.5 hours' reaction with trifluoroacetic acid (TFA)/H_2O/thioanisole/1,2-ethanedithiol/phenol (10 mL/0.5mL/0.5 mL/0.25 mL/750 mg). The $p13_{[9-22]}$ peptides were purified by reverse phase high performance liquid chromatography (RP-HPLC) on a Waters prepNova-Pak HR C18 column (Waters, Milford, MA).

Full-length p13 (87-mer) was synthesized on 4-hydroxymethylphenoxyacetyl PEGA resin (Novabiochem). Cleavage was performed by reacting the peptidyl-resin

with 95% TFA/1,2-ethanedithiol for 3 hours. Crude peptide was subsequently purified by two chromatographic steps on Waters preparative C8 (Xterra MS C8) and C18 (prepNova-Pak HR C18) RP-HPLC columns.

Molecular masses of all peptides were confirmed by mass spectroscopy.

3.8 Preparations of cytosolic and mitochondrial extracts from Jurkat-T cells

Fifty millions Jurkat-T cells were washed in PBS, resuspended in 1 ml of TES buffer (10 mM TES, 0.5 mM EGTA pH 7.4, 300 mM sucrose), and incubated on ice for 1 hour in the presence of 10 μM cytocalasin B, in order to disrupt the cytoskeleton. Cells were homogenized with a Potter homogenizer and centrifuged at 600 g for 10 min at 4 °C. The supernatant (S1) was collected, and the pellet was resuspended in 1 ml of TES buffer, re-homogenized, and centrifuged as above. The second supernatant (S2) and supernatant S1 were centrifuged as above to remove the pellet constituted by nuclei and cell debris. The resulting supernatants were centrifuged at 7,000 g for 10 minutes at 4 °C to recover mitochondria. After this centrifugations, the supernatants (the cytosolic fractions) were collected, and the mitochondrial pellets were resuspended together in 50 μl of TES buffer. The protein concentration of the mitochondrial and the cytosolic fractions was determined by Bradford Assay (Coomassie Plus Kit, Pierce). Western blotting analysis was performed using 50 and 100 ug of the preparations to assess the purity of the extraction.

3.9 *In vitro* phosphorylation assay on p13WT$_{[9-22]}$ and p13S15A$_{[9-22]}$ using purified PKC

The synthetic peptides p13WT$_{[9-22]}$ (RVWTESSFRIPSLR) or p13S15A$_{[9-22]}$ (RVWTESAFRIPSLR) were incubated at a final concentration of 300 μM with 17.5 ng of purified PKC from rat brain (Calbiochem, cod. 539494: ≥1000 units/mg protein, one unit being defined as the amount of enzyme that will transfer 1.0 nmol phosphate to histone III-S per min at 22°C, pH 7.4) in a 30 μl volume containing 50 mM Tris-HCl pH 7.5, 10 mM $MgCl_2$, 0.6 mM $CaCl_2$, 0.1 mg/ml phosphatidylserine (Sigma), and 20 μM [γ–^{33}P]ATP (specific radioactivity 2,000 cpm/pmol). The reaction mixture was incubated for 30 min at 37 °C and stopped by cooling on ice and absorption on phosphocellulose p81 filters paper. Filters were washed three

times with 75 mM phosphoric acid, dried, and counted in a scintillation counter. Final data reported in Figure 6 represents the means from two experiments.

3.10 *In vitro* phosphorylation assay on p13WT$_{[9-22]}$ and p13S15A$_{[9-22]}$ using lysates from Jurkat T-cells as a source of kinases

Reaction conditions for peptide phosphorylation experiments were as follows: p13$_{[9-22]}$ peptides, at the final concentration of 500 μM, were incubated with 1 μg of Jurkat T-cell lysate (mitochondrial or cytoplasmic fraction) in a 30 μl volume containing 50 mM Tris-HCl pH 7.5, 10 mM $MgCl_2$, 0.6 mM $CaCl_2$, 0.1 mg/ml phosphatidylserine (Sigma), phosphatase inhibitor cocktails 1 and 2 (Sigma), and 50 μM [γ–^{33}P]ATP (specific radioactivity 2,000 cpm/pmol). The reaction mixture was incubated for 5 min at 37 °C and stopped by cooling on ice and absorption on phosphocellulose p81 filters paper. Filters were processed as described above. washed three times with 75 mM phosphoric acid, dried, and counted in a scintillation counter. Final data reported in Figure 7 represent the means from four independent experiments.

3.11 *In vitro* phosphorylation assay on p13$_{[1-87]}$ using lysates from Jurkat T-cells as a source of kinases

Phopshorylation assays on full-length p13 (final concentration 3.2 μM) were carried out as described in Section 3.10. The reactions were incubated for 10 min at 37 °C and stopped by addition of 5X Laemmli loading buffer, followed by SDS−PAGE [13.5% Bis-Tris Gel, MES-SDS running buffer added with 5 mM sodium bisulfite (NuPAGE® Technical Guide, Invitrogen)]. Proteins were transferred to polyvinylidene fluoride (PVDF) membrane (Amersham Biosciences) and analyzed by immunoblotting and autoradiography (Kodak 1D and Optiquant, PerkinElmer Cyclone Plus Storage Phosphor System).

3.12 Two-dimensional gel electrophoresis

Jurkat T-cells were transfected by electroporation as described in Section 3.4 with either 3 μg of pSGp13 plus 1.5 μg of pLcxl or with 1.5 μg of pLcxl alone.

Twenty-four hours after electroporation cells were collected in aliquots of 10 x 10^6 cells, washed in PBS, and frozen at -80 °C.

Isoelectric focusing (IEF) was performed using a IPGphor system and 13-cm gel strips with a pH range of 3-11 (3-11 NL, GE Healthcare).

Aliquots of 10 x 10^6 Jurkat T-cells were lysed in 250 µl rehydration solution (8 M urea, 2% CHAPS, 0.5% IPG buffer 3-11 NL, 12 µl/ml DeStreak Reagent, a trace of bromophenol blue) and applied to the strips in the IPGphor unit. After 12 hours rehydration, IEF was run using a stepwise voltage-increase procedure: 500 V for 500 V-hours; 1,000 V for 1,000 V-hours; 8,000 V for 16,000 V-hours, corresponding to a total of 17,500 V-hrs. After IEF, the strips were equilibrated for 15 minutes in SDS equilibration buffer (50 mM Tris-HCl pH 8.8, 6 M urea, 30% glycerol, 2% SDS), supplemented with 10 mg/ml dithiothreitol (DTT) for 15 minutes, followed by a second 15-minutes equilibration step in the same buffer supplemented with 25 mg/ml iodoacetamide.

Strips were then subjected to SDS- PAGE 1-mm thick 15% polyacrylamide gels.

3.13 Immunobloting

After completing the second-dimension run, proteins were transferred to nitrocellulose membrane (Amersham Biosciences). Membranes were blocked for 1 h with 3% bovine serum albumin (BSA, Sigma) prepared in phosphate-buffered saline (PBS) and 0.05% Tween 20, washed with PBS-Tween 20 and incubated with a primary antibody for 2 hours followed by two washes, incubation with the secondary antibody for 1.5 hours, and two final washes. Rabbit polyclonal antibody raised against the synthetic protein $p13WT_{[1-87]}$ (supplied by Prof. O. Marin) and horseradish peroxidase-conjugated anti-rabbit secondary antibody (Pierce) were used. Blots were developed using Supersignal chemiluminescence reagents (Pierce) and analyzed with a BioRad ChemiDoc XRS imager.

3.14 Analysis of the mitochondrial localization of p13

HeLa-Tat cells were seeded at a density of 75,000 cells/ml onto 35 mm plates, cultured for 24 hours, and then transfected with a pSG plasmid expressing either wild-type (pSGp13) or mutant (pSGp13S15D and pSGp13S15A) p13 using Fugene 6 reagent (Roche). Twenty-four hours after transfection, the cells were washed in DMEM and fixed in 3.7% formaldehyde in complete DMEM for 20 minutes in order to maintain the mitochondrial morphology. Cells were permeabilized in 0.1% Nonidet P-40-PBS for 10 minutes, washed twice with PBS, and incubated with rabbit

polyclonal anti-p13 and goat anti-Hsp60 (Santa Cruz) for 45 minutes at 37 °C. After two washes with PBS, cells were subjected to a 30 minute-incubation with Alexa 488-conjugated anti-rabbit antibody and Alexa 546-conjugated anti-goat antibody at 37 °C (Molecular Probes). Fluorescent signals were analyzed by using an LSM510 laser scanning microscope equipped with argon (488 nM) and Helium Neon (543 nm) laser sources and quantitated by using the "Histogram" software (Zeiss). Approximately 15 cells from three different randomly selected fields were measured for each experimental group. Expression levels of p13 proteins from at least three independent experiments were normalized to the respective mean value of fluorescence intensity of p13. Hsp60 is a mitochondrial matrix protein and was used as marker of mitochondrial localization. By using the Zeiss Histogram software the colocalization indexes between the two signals (which are detected in channels 1 and 2, for Hsp60 and p13 respectively) were calculated for single cells. The colocalization index 1 (CI1) expresses a measure of the mitochondrial "filling" with p13 and is the relative number of the colocalizing p13-Hsp60 pixels, as compared to the total number of Hsp60 pixels above threshold. Colocalization index 2 (CI2), which indicates the mitochondrial localization of p13, is the ratio between the colocalizing p13-Hsp60 pixels and the total number of p13 pixels above threshold. The CI values can range between 0 and 1, according to increasing levels of colocalization between the pixels of the two channels (0 = no colocalization; 1= all pixels colocalize).

The following formulas express CI1 and CI2:

$CI1 = pixels_{Ch1,\ coloc\ with\ Ch2} / pixels_{Ch1,\ total}; = pixels_{Hsp60,\ coloc\ with\ p13} / pixels_{Hsp60,\ total};$

$CI2 = pixels_{Ch2,\ coloc\ with\ Ch1} / pixels_{Ch2,\ total} = pixels_{p13,\ coloc\ with\ Hsp60} / pixels_{p13,\ total}$

The normalized p13 fluorescence intensity values were used to separate cells into 4 groups with different levels of p13 expression; mean CI values in these expression groups were plotted. Statistical analysis was carried out using the Student's T test.

4. RESULTS

4.1 Effects of p13 on mitochondrial membrane potential

Previous studies carried out using isolated mitochondria demonstrated that p13 induces a K^+ influx resulting in depolarization and increased ROS production; these alterations in turn lower the opening threshold of the permeability transition pore in isolated mitochondria (Silic-Benussi et al., 2009). These effects were dependent on the presence of four arginines (22, 25, 29 and 30) in the functional α-helical domain spanning amino acids 21-30 (D'Agostino et al., 2002; Silic-Benussi et al., 2009).

In the present work we tested the effects of p13 in living cells by employing plasmids expressing GFP-tagged wild-type p13 (p13WT-GFP) or a mutant of p13 in which the critical arginines were substituted with glutamines (p13RQ-GFP). $\Delta\psi$ was measured using TMRM, a fluorescent lipophilic cation that accumulates in mitochondria in a $\Delta\psi$-dependent manner. The fluorescence intensity of TMRM in individual p13-expressing cells (i.e., those with a mitochondrial GFP signal) was measured using laser scanning microscopy. To confirm the potential-dependent staining of TMRM, cells were incubated with 1 μM carbonylcyanide p-trifluoromethoxyphenylhydrazone (FCCP), a protonophore that collapses the $\Delta\psi$. This treatment resulted in a loss of TMRM fluorescence, thus confirming the probe's dependence on $\Delta\psi$ and indicating that the assay was carried out below the quenching threshold of the probe.

Figure 4 shows a quantitative analysis of the effects of p13 on cells expressing different levels of the protein, measured as GFP fluorescence intensity: Panels A and B show TMRM-labelled cells with low-intermediate levels of p13WT-GFP and p13RQ-GFP, respectively, and Panels C and D show cells expressing higher levels of the proteins. The tables on the right-hand side of the figure report the mean fluorescence intensities of GFP and TMRM in the cells analyzed, indicated by numbers. The scatter plots show TMRM fluorescence intensity (y axis) and GFP fluorescence intensity (x axis) measured within a single cell, indicated by a white line. Cells expressing low to intermediate levels of p13WT-GFP varied in terms of $\Delta\psi$ (see tables in Panels A and B), while cells expressing p13RQ-GFP invariably maintained $\Delta\psi$. These observations indicated that p13 was essential but not sufficient for depolarization, suggesting that its function might be subjected to regulation. In contrast, cells expressing high levels of p13WT-GFP (Panel C) exhibited a marked

reduction in TMRM. No reduction in TMRM fluorescence was observed in cells expressing high levels of p13RQ-GFP (Panel D).

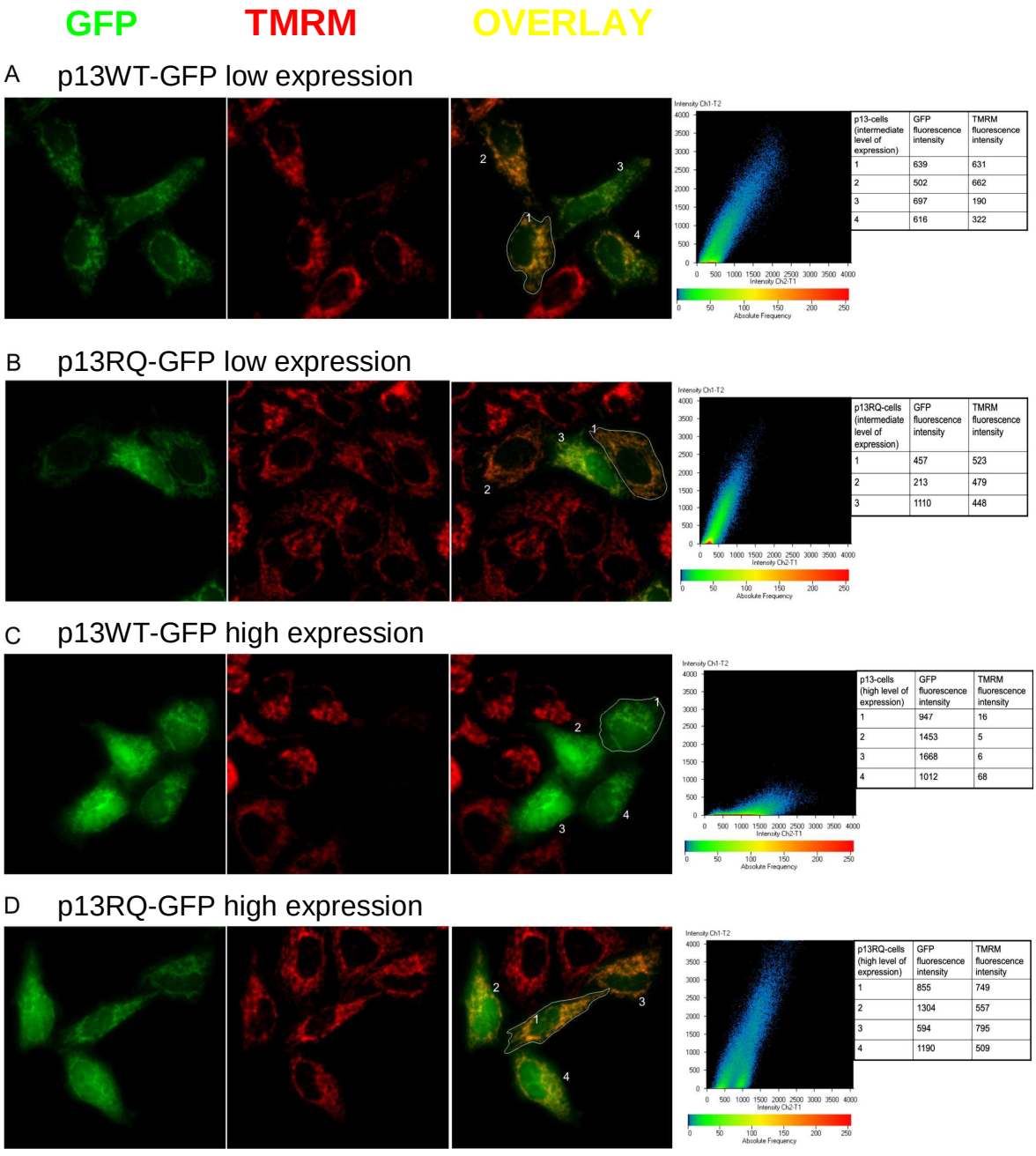

Figure 4: Effects of p13 on Δψ in cells. HeLa-Tat cells were transfected with wild-type p13WT-GFP (Panels 1A and 1C) or p13RQ-GFP (Panels 1B and 1D). Eighteen hours later, cells were incubated with 5 nM TMRM and 20 μg/ml verapamil for 30 minutes, and fluorescence intensities of TMRM and GFP were detected by laser scanning microscopy and analyzed as described in Materials and Methods. Images show the GFP, TMRM and overlay signals (20X magnification) of cells with low expression levels (Panels 1A and 1B) and with high expression levels (Panels 1C and 1D). The scatter plots show TMRM fluorescence intensity plotted against GFP fluorescence intensity measured in the cell selected by the white line. Tables report GFP and TMRM fluorescence measured in the numbered cells.

The effect of p13-GFP on $\Delta\psi$ in living cells was further analyzed using data collected from four independent experiments, with at least 100 cells expressing p13WT-GFP or p13RQ-GFP at different levels analyzed in each experiment. TMRM signals measured in cells expressing p13WT-GFP or p13RQ-GFP were scaled against the mean TMRM fluorescence intensity measured in non-transfected cells (i.e., cells without a detectable GFP signal). Fluorescence intensity values measured for p13RQ-GFP were scaled against the mean fluorescence intensity of p13WT-GFP. Results of this analysis are shown in Figure 5A, where normalized GFP fluorescence intensity values were used to separate cells into five groups with different levels of p13 expression, and mean TMRM fluorescence values for each group were plotted. This analysis revealed that cells expressing lower levels of p13WT-GFP exhibited mean normalized values of $\Delta\psi$ similar to those recorded in cells expressing comparable levels of p13RQ-GFP. However, as p13WT-GFP expression levels increased, mean normalized values of $\Delta\psi$ progressively diminished. In contrast, no significant change in $\Delta\psi$ was observed as p13RQ-GFP levels increased. Statistical analysis demonstrated highly significant differences between wild-type and mutant p13-expressing cells in the intermediate ($p_{1.5\text{-}1.99} = 0.0063$) and high expression groups ($p_{\geq 2} = 2.92 \times 10^{-6}$).

As shown in Figure 5B, the mean values of TMRM fluorescence of the WT vs. mutant p13-expressing cells were significantly different even after pooling all data irrespective of expression levels ($p = 4.28 \times 10^{-5}$). The mean expression level of p13RQ-GFP was slightly lower than that of p13WT-GFP, but this difference was not statistically significant ($p = 0.0771$, Figure 5C).

Taken together, these observations indicate that the effect of p13 on $\Delta\psi$ in living cells is dose-dependent, as observed in previous assays carried out using synthetic p13 and isolated mitochondria (Silic-Benussi et al., 2009).

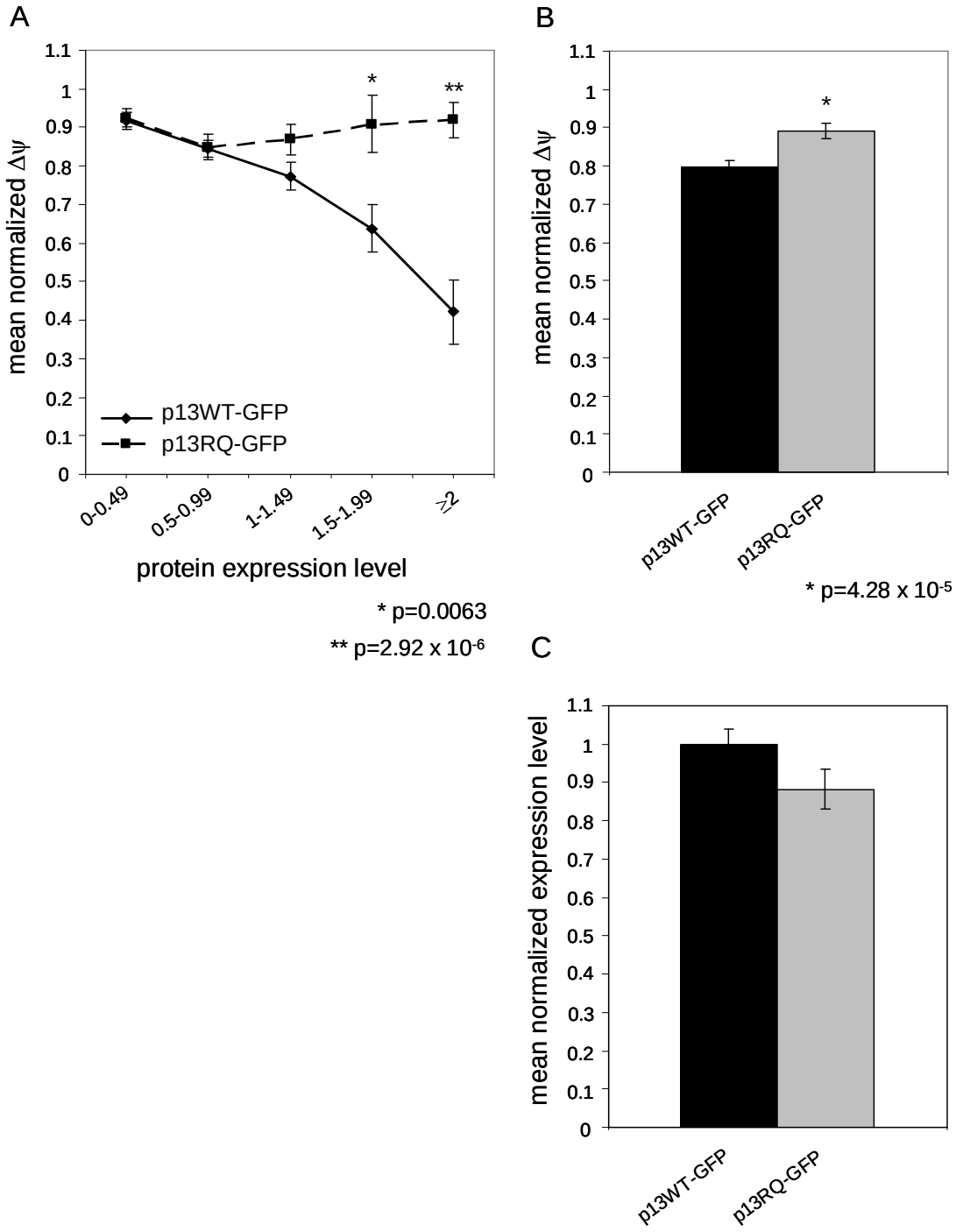

Figure 5: Effect of p13 on Δψ in HeLa cells. Panel A shows TMRM fluorescence plotted against p13 expression ranges, normalized as indicated in Materials and Methods. The data were obtained from the analysis of 487 p13WT-GFP and 409 p13RQ-GFP cells. The asterisks indicate a significant difference calculated with Student's T test: $p_{1.5\text{-}1.99} = 0.0063$, and $p_{>2} = 2.9260 \times 10^{-6}$. The plot in Panel B was generated with data pooled from all analyzed cells. The Δψ is represented as the ratio between the fluorescence intensity (FI) of TMRM in p13WT- or p13RQ-expressing cells and the TMRM mean FI in non-transfected cells. Mean normalized values and standard error bars are shown. $p = 4.28 \times 10^{-5}$. In C the mean normalized expression levels and standard error bars are represented (p=0.0771).

The effects of p13 on Δψ were also tested in Jurkat T-cells, as CD4+ T-cells are the natural target of HTLV-1 infection (Manel et al., 2005) Jurkat T-cells were transfected by electroporation with plasmids expressing p13WT-GFP or p13RQ-GFP, and incubated in HEPES-buffered complete RPMI with the potential-dependent probe TMRM and verapamil for 30 minutes at 37 °C. The fluorescence intensities of TMRM and of GFP were analyzed by flow cytometry. To confirm the potential-dependent staining of TMRM, cells were incubated with 1 μM FCCP, which resulted in a loss of TMRM fluorescence, thus confirming the probe's dependence on Δψ. In this assay the percentage of "polarized" cells (p13WT-GFP- or p13RQ-GFP-expressing cells with a Δψ within the range of Δψ measured in control cells) out of the total number of cells analyzed for sub-groups of p13 expression, was calculated (Figure 6). Cells were clustered into six groups based on their p13 expression levels (values of GFP fluorescence intensity:10-49; 50-99; 100-199; 200-299; 300-399; 400-500) in order to determine the percentage of polarized cells for each range of expression. Results in Figure 6 demonstrated that p13WT-expressing cells showed a lower percentage of polarized cells compared to p13RQ-expressing cells, for each range of expression, suggesting that p13 expression induces mitochondrial depolarization in higher number of cells compared to p13RQ. This difference was significant in the sub-group 50-99 ($p_{50-99} = 0.0284$), and at high levels of expression ($p_{400-500} = 0.0122$).

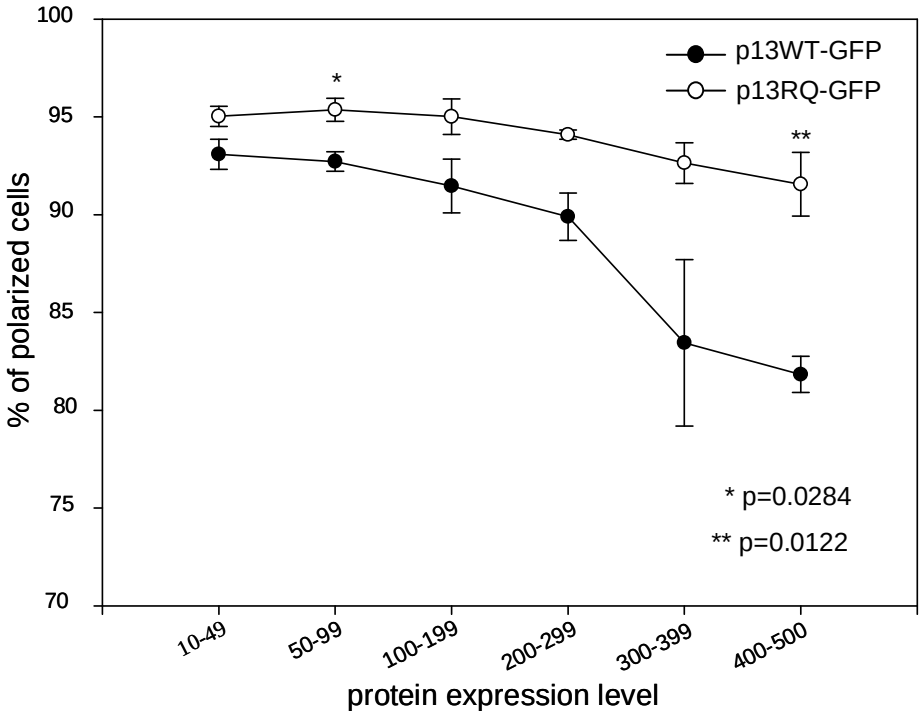

Figure 6: Effects of p13 on Δψ in Jurkat T-cells. The graph shows the percentage of depolarized cells plotted against p13 expression ranges (GFP fluorescence intensity), as indicated in Materials and Methods. The data were obtained from three independent experiments. The asterisks indicate a significant difference calculated by Student's T test: $p_{50\text{-}99} = 0.0283$; $p_{400\text{-}500} = 0.0122$. Mean values and standard error bars are represented.

4.2 Effects of p13 on Ca^{2+} uptake by mitochondria

As mitochondrial Ca^{2+} uptake is known to be driven by $\Delta\psi$ (Pinton et al., 2008), we next investigated whether the effects of p13 on $\Delta\psi$ translate in changes in mitochondrial Ca^{2+} homeostasis. This was tested by transfecting HeLa cells with wild-type p13, a panel of p13 arginine mutants (p13RQ, p13RP, p13RAL), or mitochondrial-targeted GFP (serving as a control mitochondrial protein) together with an aequorin probe targeted to the mitochondria. After aequorin reconstitution with coelenterazine, cells were challenged with 100 μM histamine, an agonist that acts on G-coupled receptor resulting in inositol 1,4,5 trisphosphate (IP3) production and Ca^{2+} release from intracellular stores. This assay was performed three times, and results were assessed by measuring the Ca^{2+} peak amplitude.

As shown in Figure 7A, p13 caused a mean 56% reduction in the mitochondrial Ca^{2+} peak amplitude compared to the control (peak amplitude: p13 = 27±4 μM; control = 62±3 μM; $p = 3 \times 10^{-6}$). In contrast, the arginine mutants p13RQ and p13RAL did not significantly affect mitochondrial Ca^{2+} uptake (peak amplitude: p13RQ = 69±4 μM; p13RAL = 63±4 μM). p13RP produced a modest but statistically significant increase in mitochondrial Ca^{2+} content (peak amplitude: p13RP = 74±5 μM, p = 0.04). To investigate whether p13's effects on mitochondrial Ca^{2+} content could also influence cytosolic [Ca^{2+}] or could be dependent on a change in Ca^{2+} release from the ER, we measured the effects of p13 on cytosolic and ER [Ca^{2+}] using aequorins targeted to these compartments. Results of three independent experiments showed that p13 did not significantly affect cytosolic [Ca^{2+}] (Figure 7B, peak amplitudes: control = 2.37±0.07 μM; p13 = 2.30±0.12 μM; p13RQ = 2.54±0.06 μM; p13RP = 2.40±0.10 μM; p13RAL = 2.22±0.09 μM) or ER Ca^{2+} filling (Figure 7C, steady state: control = 442±13 μM; p13 = 460±27 μM). Similar to wild-type p13, the arginine mutants p13RP and p13RAL did not differ substantially from the control (steady state: p13RP = 500±20 μM; p13RAL = 489±18 μM), while the glutamine mutant induced slightly higher ER loading compared to the control (steady state: p13RQ = 520±20 μM, p = 0.01).

Taken together, these results demonstrate that p13 specifically reduces mitochondrial Ca^{2+} uptake. The observation that the arginine mutants did not negatively influence mitochondrial Ca^{2+} uptake strongly suggests that this effect is tightly linked to the ability of p13 to induce mitochondrial K^+ influx and

depolarization. It is also possible that p13's effects on Ca^{2+} homeostasis might result from the protein's ability to promote mitochondrial fragmentation (Ciminale et al., 1999).

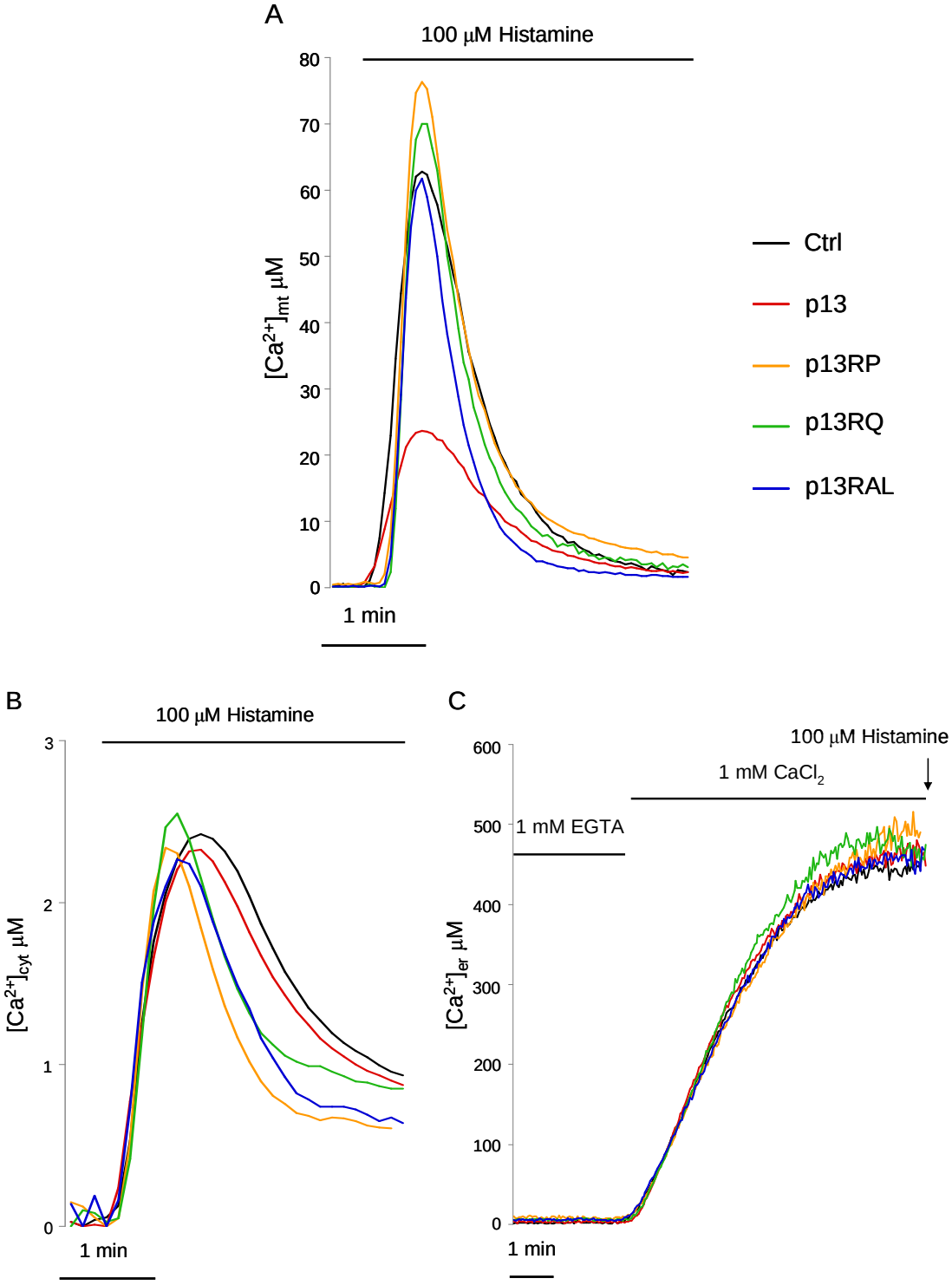

Figure 7: Measurement of Ca^{2+} content in mitochondria (mt), cytosol (cyt), and endoplasmic reticulum (er) of p13-expressing cells. [Ca^{2+}] in mitochondria (A), cytosol (B), and ER (C) of HeLa cells expressing control (mtGFP), wild-type p13, or arginine mutants (p13RP, p13RQ, p13RAL) was analyzed using aequorin probes as described in Materials and Methods. After aequorin reconstitution, cells were challenged with 100 µM histamine, as indicated in the graphs. The traces show resulting

measurements of [Ca^{2+}] as a function of time, and are representative of three independent experiments.

4.3 *In silico* prediction of phosphorylation sites in p13

Based on the heterogeneity of the effects of p13 on $\Delta\psi$ (see above), we hypothesized the existence of a regulatory mechanism of p13 function. One obvious possibility is that p13 function could be regulated by phosphorylation. We therefore analyzed the amino acid sequence of p13 (Figure 8A) using programs to predict potential phosphorylation sites.

The p13 sequence was first analyzed using the PROSITE prediction server (www.expasy.ch) (Falquet et al., 2002), which identifies PKC phosphorylation sites. As shown in figure 8B, serines in the positions 15, 20, and 45 were indicated as putative PKC target sites, according to the consensus pattern [ST]-X-[RK] where S or T is the phosphorylation site, followed by a C-terminal basic residue (R or K) in position +2 (Kennelly and Krebs, 1991; Nishikawa et al., 1997). In this case S15, S20, S45 are followed by arginine at positions 17, 22, and 47 respectively (sequences: SFR, SLR, SSR).

p13 sequence was also scanned using NetPhosK (www.cbs.dtu.dk/services/NetPhosK), which attributes a kinase-specific score, ranging from 0 to 1, to a putative phosphorylation site (Blom et al., 2004). Unlike PROSITE, NetPhosK is a method based on neural network. A series of kinase-specific sites was identified by NetPhosK, as listed in the Figure 8C, and many of them were predicted to be PKC target sites (S14, S15, T38, T44, S71, T72).

After comparing the results of the two analyses we decided to focus our studies on S15, because it was identified by both predictions and because of its key location in the proximity of the α-helical functional domain (spanning residue 21-30) (D'Agostino et al., 2002), suggesting that it might be involved in the modulation of protein function or localization.

A

MLIISPLPRV WTESSFRIPS (1-20)
LRVWRLCARR LVPHLWGTMF (21-40)
GPPTSSRPTG HLSRASDHLG (41-60)
PHRWTRYQLS STVPYPSTPL (61-80)
LPHPENL (81-87)

B

PKC sites (PROSITE)

Position	
S-15	**S**FR
S-20	**S**LR
S-45	**S**SR

C

Kinase-Specific sites (NetPhospK)

Position	Context	Kinase	Score
T-12	PRVW**T**ESSF	PKG	0.51
S-14	VWTE**S**SFRI	PKC	0.69
S-15	WTES**S**FRIP	PKC	0.58
S-20	FRIP**S**LRVW	PKA	0.66
T-38	HLWG**T**MFGP	PKC	0.63
T-38	HLWG**T**MFGP	cdc2	0.56
T-44	FGPP**T**SSRP	PKC	0.59
S-46	PPTS**S**RPTG	cdc2	0.54
S-56	LSRA**S**DHLG	PKA	0.64
T-65	PHRW**T**RYQL	PKA	0.64
S-70	RYQL**S**STVP	cdc2	0.57
S-71	YQLS**S**TVPY	PKC	0.76
S-71	YQLS**S**TVPY	cdc2	0.51
T-72	QLSS**T**VPYP	PKC	0.71
T-72	QLSS**T**VPYP	cdc2	0.56
T-78	PYPS**T**PLLP	p38MAPK	0.54
T-78	PYPS**T**PLLP	GSK3	0.51
T-78	PYPS**T**PLLP	cdk5	0.64

Figure 8: p13 amino acid sequence and phosphorylation site predictions. A. p13 amino acid sequence: underlined is the MTS (21-30); B. Prediction of PKC phosphorylation sites by PROSITE, according to the consensus sequence [ST]X[RK]; C. Prediction of kinase-specific phosphorylation sites by NetPhosK, indicating the score for each kinase.

4.4 *In vitro* phosphorylation of p13WT$_{[9-22]}$ and p13S15A$_{[9-22]}$ by isolated PKC and lysates from Jurkat T-cells

In order to confirm that S15 might be a PKC-specific target site, we performed preliminary *in vitro* phosphorylation assays using purified PKC from rat brain (Calbiochem), and the synthetic peptides p13WT$_{[9-22]}$ (RVWTESSFRIPSLR) and p13S15A$_{[9-22]}$ (RVWTESAFRIPSLR), in which S15 was substituted with alanine, a non-phosphorylatable amino acid as a negative control. These peptides simplified the *in vitro* phosphorylation analysis (described in Materials and Methods), as they contained only three other possible phosphorylation sites (T12, S14, and S20).

After incubation of the substrates and the kinases in the presence of [γ–^{33}P]ATP, the reaction mixture was absorbed on phosphocellulose p81 paper, and counted in a scintillation counter. As shown in Figure 9A we found that p13WT$_{[9-22]}$ is more efficiently phosphorylated by PKC (147.79 pmol/min), compared to p13S15A$_{[9-22]}$ (50.36 pmol/min). The phosphorylation of the positive control Histone IIIs confirmed the activity of the enzyme in the assay (data not shown). After blank subtraction and expressing data as percentage of p13WT$_{[9-22]}$ phosphorylation, the

wild-type peptide was found to be a 3-fold better PKC sustrate than the mutant peptide, confirming that S15 is the major PKC site in the context of this peptide (Figure 9B).

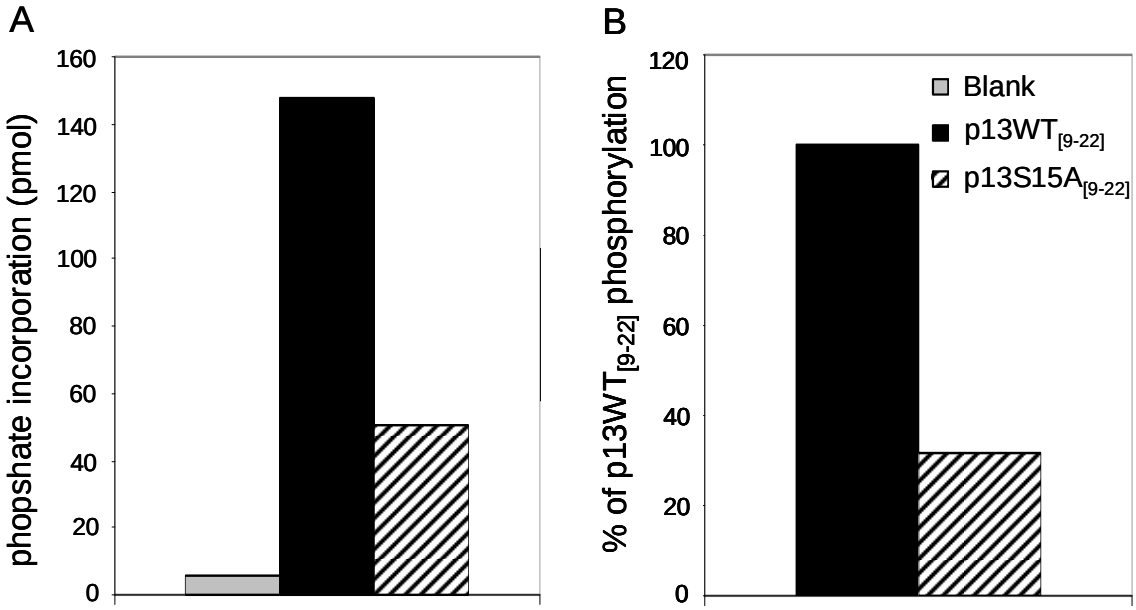

Figure 9: The phosphorylation of peptides p13WT$_{[9-22]}$ and p13S15A$_{[9-22]}$ by purified PKC from rat brain. A. The graph represents the phosphate incorporation of p13WT$_{[9-22]}$ compared to p13S15A$_{[9-22]}$, The synthetic substrates were incubated with 17.5 ng of PKC as detailed in Materials and Methods. Background (blank) was evaluated by performing the phosphorylation reaction in the absence of the peptides. In graph B, the background phopshorylation measured in the blank was subtracted and phosphorylation measured for the wild-type peptide was set at 100%.

We next analyzed the phosphorylation of the 9-22 peptides by using Jurkat T-cell lysates as a source of kinases in order to investigate whether a cellular PKC (or other cellular kinases) expressed in T-cells might be involved in S15 phosphorylation. Jurkat T-cells were chosen as a model system because *in vivo* HTLV-1 infection preferentially targets CD4+ T-lymphocytes (Manel et al., 2005). Mitochondrial and cytoplasmic lysates were obtained from 50 x 10^6 cells, quantified by Bradford assay (Pierce) and analyzed by western blot for mitochondrial and cytoplasmic markers (data not shown) to test the purity of the preparations. Time of incubation and lysates quantity used in the phosphorylation assays were optimized by selecting the conditions that allow a linear phosphate incorporation by the wild-type peptide and minimal nonspecific phosphate incorporation in the absence of the peptides (blank).

Following a 5-minute incubation in the presence of 1 µg of each cellular lysate, we found that p13WT$_{[9-22]}$ was significantly more highly phosphorylated compared

to p13S15A$_{[9-22]}$ by both extracts, as demonstrated in Figure 10, which shows the rate of phosphorylation and the error bars of four independent experiments. In detail, in the presence of the mitochondrial fraction (Figure 10A) the phosphorylation of p13WT$_{[9-22]}$ was 3.04 pmol/min/μg of lysate compared to 1.84 pmol/min/μg of lysate for p13S15A$_{[9-22]}$ ($p = 0.0286$). Expressed as percentage of phosphorylation of the wild-type after blank subtraction (phosphate incorporation of blank = 0.69 pmol/min/μg of lysate; Figure 10B), the phosphorylation of the p13S15A mutant was 48.82% of that of the wild type.

Incubation of the peptides with 1 μg of cytoplasmic lysate (Figure 10C) yielded higher rates of phosphorylation compared to those obtained with the mitochondrial lysate. On the contrary, the blanks were very similar (0.67 pmol/min/μg of lysate). After blank subtraction the degree of phosphorylation of p13S15A$_{[9-22]}$ was 61.53% (4.44 pmol/min/μg of lysate) of that of the p13WT$_{[9-22]}$ (6.79 pmol/min/μg of lysate). The difference in phosphorylation levels was statistically significant ($p = 0.036$, Figure 10D).

The residual phosphorylation of the alanine mutant peptide using mitochondrial and cytoplasmic fractions might be due to the contribution of the three other possible target sites in the 9-22 peptides (T12, S14, and S20). Nevertheless, the consistent reduction in the phosphorylation of p13S15A$_{[9-22]}$ (approximately 50% and 40%, for mitochondrial and cytoplasmic extracts, respectively) indicates that S15 might be a major kinase target site in the context of residues 9-22.

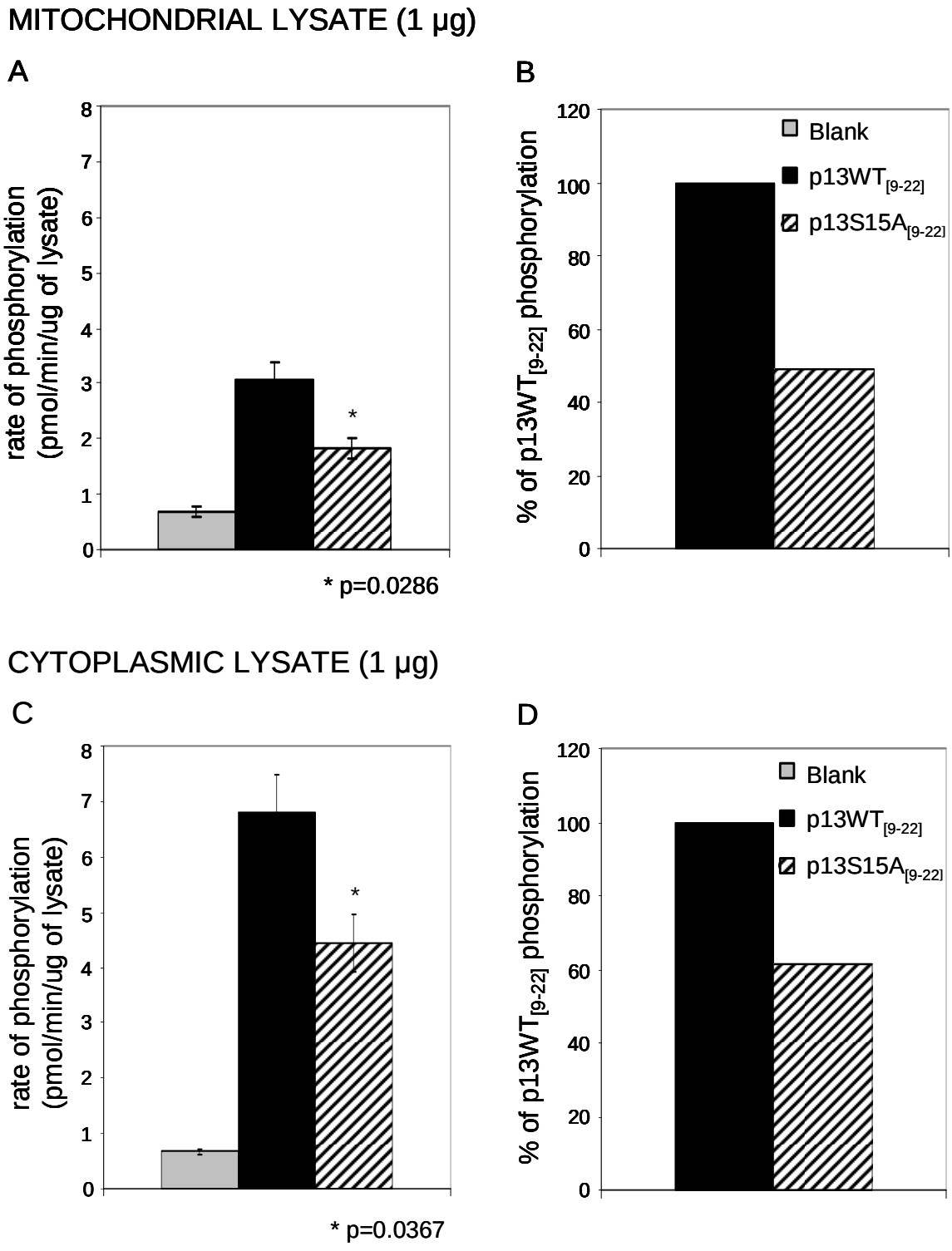

Figure 10: Phosphorylation of peptides p13WT$_{[9-22]}$ and p13S15A$_{[9-22]}$ by mitochondrial and cytoplasmic lysates from Jurkat T-cells. The graphs in A and C represent phosphate incorporation of p13WT$_{[9-22]}$ compared to p13S15A$_{[9-22]}$, expressed as pmol/min/ug of lysate. The reaction mix was incubated for 5 minutes as described in Materials and Methods. Backround (blank) was evaluated by performing the phosphorylation reaction in the absence of the peptides. The graphs in B and D show phosphate incorporation expressed as the percentage of the phosphorylation of p13WT$_{[9-22]}$, set at 100%, after background subtraction.

4.5 *In vitro* phosphorylation of p13[1-87] by Jurkat T-cells lysates

In order to analyze the phosphorylation of p13 in the context of the full-length protein, we performed *in vitro* phosphorylation assay by using synthetic $p13_{[1-87]}$ and Jurkat T-cell mitochondrial and cytoplasmic lysates (2 μg) as a source of kinases. Following a 10-minute incubation at 37 °C, the reaction was stopped by adding 5X Laemmli loading buffer and, after SDS-PAGE, samples were analyzed by western blot and autoradiography as described in Materials and Methods. Figure 11 shows the results of a representative experiment. Synthetic $p13_{[1-87]}$, which migrates at 10 kDa (monomer) and at 20 kDa (dimer), was confirmed to be phosphorylated by cellular lysates from Jurkat T-cells.

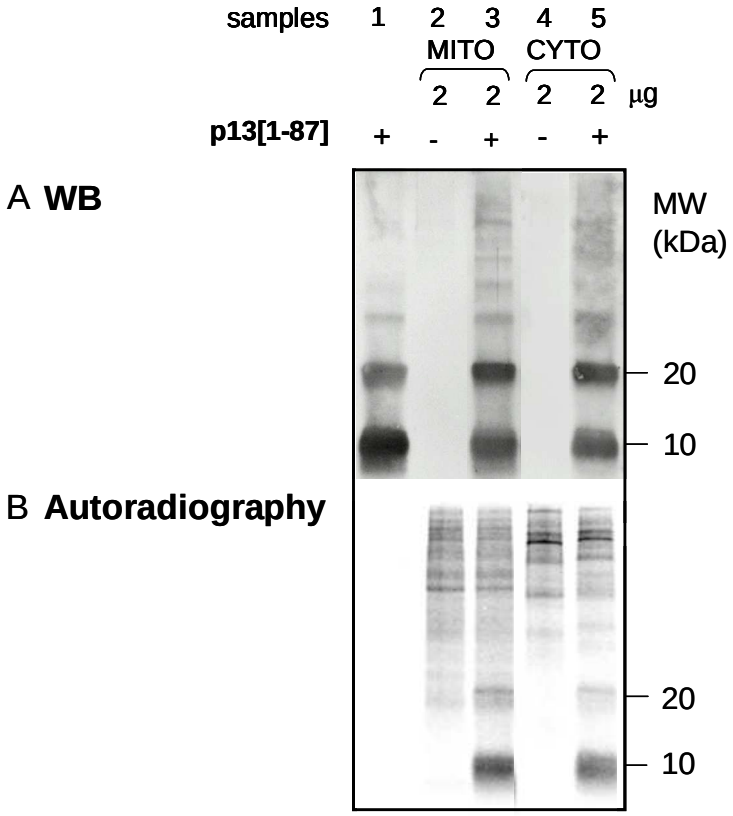

Figure 11: Phosphorylation of synthetic $p13_{[1-87]}$ by mitochondrial and cytoplasmic lysates from Jurkat T-cells. Western blot (A) and corresponding autoradiography (B) of the following samples, from right to left: 1) $p13_{[1-87]}$; 2) 2 μg of mitochondrial lysate; 3) $p13_{[1-87]}$ in the presence of 2 μg of mitochondrial lysate; 4) 2 μg of cytoplasmic lysate; 5) $p13_{[1-87]}$ in the presence of 2 μg of cytoplasmic lysate. $p13_{[1-87]}$ is significantly phosphorylated by both lysates.

4.6 Analysis of the net charge of p13 by two-dimensional gel electrophoresis

The addition of phosphates to a protein will alter its net charge toward a more acidic isoelectric point (pI). Figure 12 shows a prediction of the pI of p13 obtained using Scansite prediction software (http://scansite.mit.edu/calc_mw_pi.html) (Obenauer et al., 2003). Considering all the possible phosphorylation sites in p13's amino acid sequence (11 serines, 7 threonines, and 2 tyrosines, corresponding to a total of 20 possible phosphorylation sites) and in the presence of a corresponding number of phosphates, its pI might become significantly acidic. To examine this property of p13, we performed two-dimensional electrophoresis (i. e. separation based on net charge follwed by SDS-PAGE size separation) on p13 expressed in Jurkat T-cells. We transiently transfected Jurkat T-cells by electroporation with a plasmid encoding p13 in the presence of a plasmid coding for Tax, which enhances p13 expression. A lysate from 10 x 10^6 cells was prepared and applied to an isoelectric focusing strip covering a wide range of pH (3-11 NL), selected as the most suitable for assessing the pI of phosphorylated p13.

Phosphates	Theoretical isoelectric point
0	11.64
1	11.11
2	10.00
3	8.39
4	7.40
5	7.01
6	6.71
7	6.46
8	6.22
9	5.98
10	5.72
11	5.41
12	5.01
13	4.57
14	4.16
15	3.76
16	3.41
17	3.14
18	2.95
19	2.80
20	2.70

Figure 12: pI prediction of p13 by using Scansite prediction software. The presence of a growing number of phosphates might significantly lower the pI of p13, from 11.64, in the absence of phosphate, to 2.70, if every possible phosphorylation site were modified.

Following isoelectric focusing the strip was applied to a 15% SDS-PAGE gel; separated proteins were transferred to a filter and subjected to immunoblotting with an anti-p13 antibody. Figure 13 shows a representative result. p13 was detected as two main spots: the former is in the basic part of the gel (pH ≈ 9), while the latter showed very acidic features, localizing between pH 4 and pH 5. This result, obtained in five independent experiments, suggests that p13 is phosphorylated in Jurkat T-cells. Control 2D gels performed using lysates of Jurkat T-cells transiently transfected with the Tax plasmid alone were performed and confirmed the specificity of the signal detected for p13 (data not shown). The major spots of p13, detected at pI 9 and pI 4.5, are compatible with the presence of 2 or 3 phosphates and 12 or 13 phosphates, respectively.

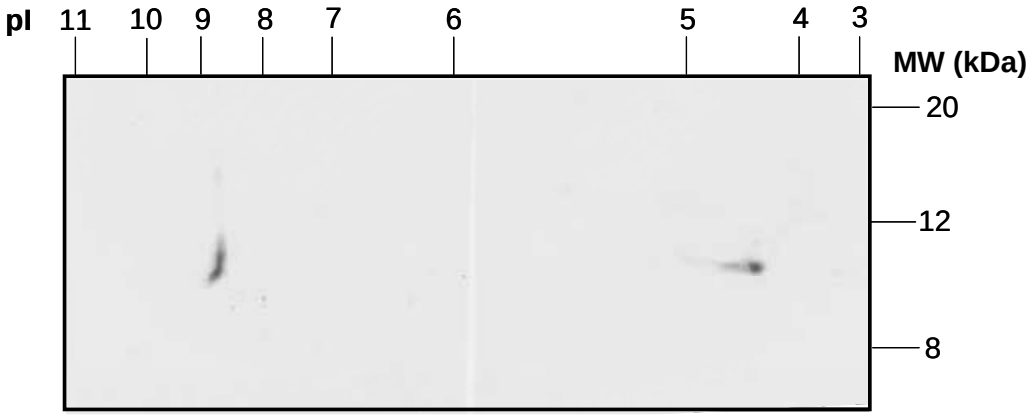

Figure 13: Immunoblot of two-dimensional electrophoretic separation of Jurkat T-cells experring p13. The pI gradient was positioned as described in "Immobiline DryStrip visualization of pH gradients (technical brochure)", GE Healthcare.

4.7 Effects of phosphomimetic and phosphoablative mutations of S15 on the intracellular localization of p13 and its effects on mitochondrial morphology

In order to analyze the functional effects of the phosphorylation of p13 in S15, we produced phosphomimetic (p13S15D) and phosphoablative (p13S15A) mutants by site-specific mutagenesis and analyzed their properties.

Intracellular localization of wild-type p13 and S15 mutants was analyzed by immunofluorescence and laser scanning microscopy using Hsp60 as a mitochondrial marker. Figure 14A shows representative immunofluorescence images of p13WT, p13S15A, and p13S15D, with p13 detected as a green signal, and Hsp60 in red. The phosphoablative mutant p13S15A exhibited a mitochondrial pattern similar to that of the wild-type protein, while the phosphomimetic mutant p13S15D exhibited a mixed

pattern of mitochondrial, nuclear and cytosolic localization. The apparent mitochondrial fragmentation was more pronounced in p13S15D-expressing cells compared to p13WT and p13S15A.

The difference in the cellular distribution was then quantitavely measured by analyzing the colocalization indexes (CI) as a function of protein expression level, using Zeiss Histogram software, at a single cell level. As described in Materials and Methods, the colocalization indexes measure the relative number of colocalizing pixels in each channel, compared to the total number of pixels above threshold. Channel 1 (Ch1) detects Hsp60, while channel 2 (Ch2) detects p13. In Figure 14B and 14C mean CI values were expressed as a function of groups of normalized expression level of the proteins. As shown in Figure 14B p13WT and p13S15A exhibited mostly a mitochondrial localization (p13: $CI2_{0\text{-}0.49} = 0.80$; $CI2_{0.5\text{-}0.99} = 0.89$; $CI2_{1\text{-}1.49} = 0.89$; $CI2_{\geq 1.5} = 0.79$; p13S15A: $CI2_{0\text{-}0.49} = 0.67$; $CI2_{0.5\text{-}0.99} = 0.88$; $CI2_{1\text{-}1.49} = 0.81$; $CI2_{\geq 1.5} = 0.76$). In contrast, p13S15D was significantly less mitochondrially-targeted, and distributed to other cell compartments, except when expressed at low levels (p13S15D: $CI2_{0\text{-}0.49} = 0.73$; $CI2_{0.5\text{-}0.99} = 0.56$ $p_{0.5\text{-}0.99} = 3.8792 \times 10^{-5}$; $CI2_{1\text{-}1.49} = 0.57$ $p_{1\text{-}1.49} = 3.0801 \times 10^{-5}$; $CI2_{\geq 1.5} = 0.57$ $p_{1\text{-}1.49} = 0.0326$). Figure 14C shows that mitochondria were similarly "loaded" with p13 and p13S15A, according to the expression level of the protein (p13: $CI1_{0\text{-}0.49} = 0.79$; $CI1_{0.5\text{-}0.99} = 0.74$; $CI1_{1\text{-}1.49} = 0.78$; $CI1_{\geq 1.5} = 0.88$; p13S15A: $CI1_{0\text{-}0.49} = 0.91$ $p_{0\text{-}0.49} = 0.0216$; $CI1_{0.5\text{-}0.99} = 0.75$; $CI1_{1\text{-}1.49} = 0.84$; $CI1_{\geq 1.5} = 0.92$). Interestingly, the phosphomimetic mutant p13S15D yielded slightly higher values for mitochondrial "loading" (p13S15D: $CI2_{0\text{-}0.49} = 0.89$ $p_{0\text{-}0.49} = 0.0317$; $CI2_{0.5\text{-}0.99} = 0.97$ $p_{0.5\text{-}0.99} = 6.8652 \times 10^{-4}$; $CI2_{1\text{-}1.49} = 0.98$ $p_{1\text{-}1.49} = 0.0023$; $CI2_{\geq 1.5} = 0.99$ $p_{1\text{-}1.49} = 1.2626 \times 10^{-4}$). Taken together, these results suggest that the phosphomimetic mutation of S15 increased p13's mitochondrial targeting, that however was associated with an extra-mitochondrial localization in the cytoplasm and in the nucleus, probably due the dramatic disruption of the mitochondrial network induced by the mutant.

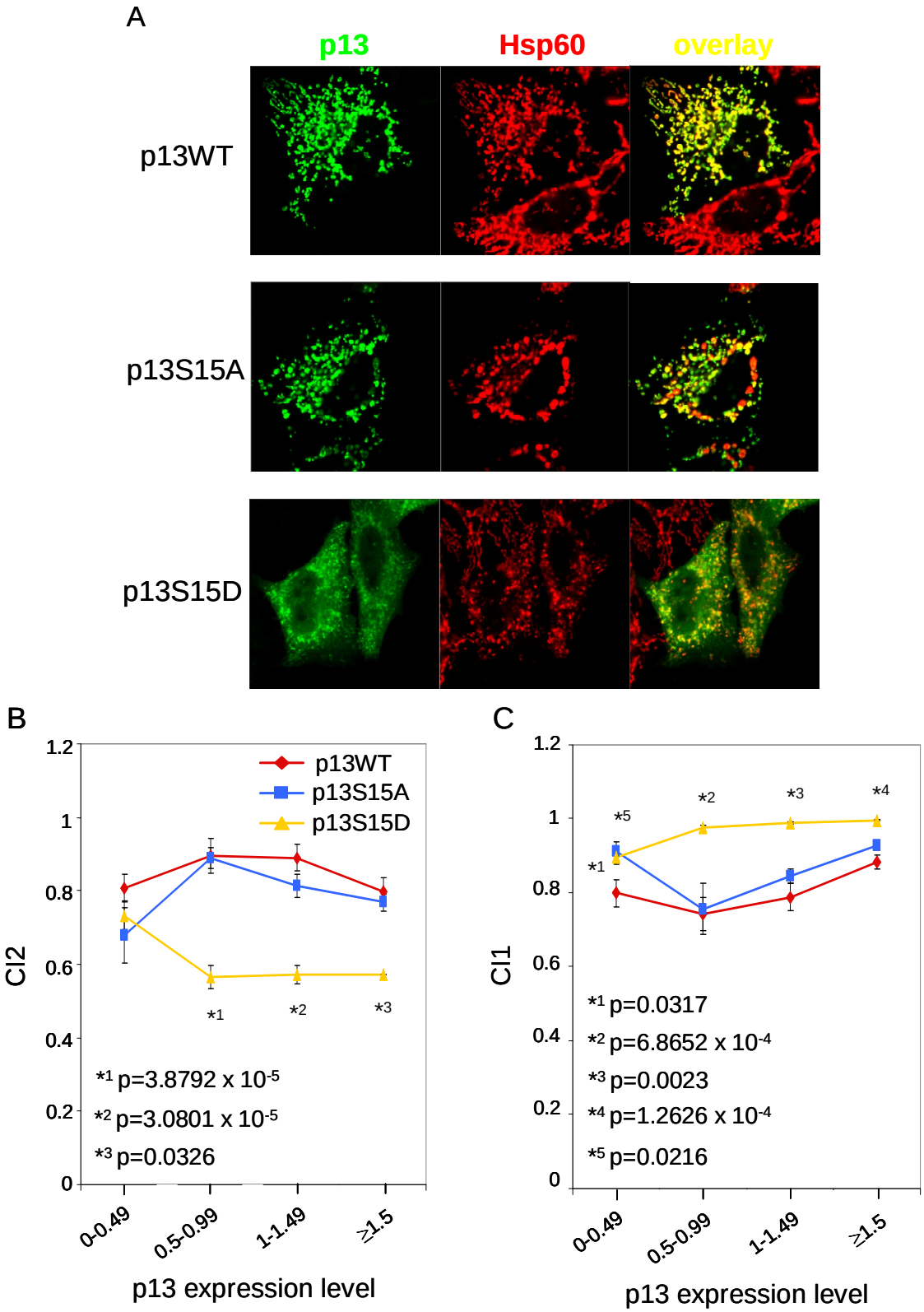

Figure 14: Mitochondrial targeting of phosphomimetic (p13S15D) and phosphoablative (p13S15A) mutants of p13. A. Representative immunofluorescence images of p13WT, p13S15A, p13S15D (in green) and the mitochondrial marker Hsp60 (in red); magnification 60X. B and C. Graphs representing CI2 and CI1 as a function of protein expression level. Data derived from the analysis of 38, 41, and 47 cells expressing p13, p13S15A, and p13S15D respectively, from 3 independent experiments. Asterisks indicate a significantive difference between the wild-type and the mutants in the respective expression level group calculated by Student's T test. Mean normalized values and standard error bars are indicated. In B: p13S1D: $p_{0.5\text{-}0.99}$ = 3.8792 x 10^{-5}; $p_{1\text{-}1.49}$ = 3.0801 x 10^{-5}; $p_{\geq 1.5}$= 0.0326. In C: p13S15A: $p_{0\text{-}0.49}$ = 0.0216. In p13S15D: $p_{0\text{-}0.49}$ = 0.0317; $p_{0.5\text{-}0.99}$ = 6.8652 x 10^{-4} ; $p_{1\text{-}1.49}$ = 0.0023; $p_{\geq 1.5}$= 1.2626 x 10^{-4}.

4.8 Effects of phosphomimetic and phosphoablative mutations on mitochondrial membrane potential

The phosphomimetic and phosphoablative mutants were used to study the possible influence of S15 on changes of $\Delta\psi$ induced by p13. HeLa-Tat cells were transfected with plasmids encoding p13-GFP, p13S15A-GFP, p13S15D-GFP, and incubated in the presence of TMRM to measure mitochondrial $\Delta\psi$ in living cells. As described in Materials and Methods, TMRM staining and GFP fluorescence were measured by laser scanning microscopy. GFP fluorescence intensity values were scaled against the mean fluorescence intensity of p13WT-GFP and grouped in four different ranges of expression. TMRM signals measured in cells expressing p13-GFP were normalized to the mean TMRM fluorescence intensity value measured in nontransfected cells (i.e., cells without a detectable GFP signal). Mean TMRM fluorescence values for each expression group were plotted. Data were collected from three independent experiments, with at least 45 cells expressing p13WT-GFP, or p13S15A-GFP, or p13S15D-GFP at different levels analyzed in each experiment.

This analysis (Figure 15A) demonstrated that the phosphomimetic mutation of S15 significantly potentiated p13's effect on $\Delta\psi$, inducing a marked depolarization at lower levels of expression compared to the wild-type protein ($p_{0.5\text{-}0.99} = 4.1198 \times 10^{-4}$) that increased at higher expression levels ($p_{1\text{-}1.49} = 6.674 \times 10^{-16}$; $p_{1.5\text{-}1.99} = 0.0015$). Interestingly, the phosphoablative mutation significantly impaired p13 function, suggesting that S15 phosphorylation might have a strong positive regulatory effect on p13 function ($p_{1.5\text{-}1.9} = 0.0418$; $p_{\geq 2} = 0.0031$). When the data were pooled together irrespective of expression levels (Figure 15B), the reduction in $\Delta\psi$ induced by p13-GFP and p13S15D-GFP was similar, while p13S15A-GFP-expressing cells maintained a significantly higher $\Delta\psi$ ($p = 1.4751 \times 10^{-4}$). The mean expression level of p13S15D-GFP was found to be significantly lower than that of p13WT-GFP ($p = 5.9425 \times 10^{-5}$, Figure 15C). It is noteworthy that transfections with p13S15D yielded relatively few cells expressing high levels of the protein. This could reflect the dramatic effects of this mutant on $\Delta\psi$, which are likely to result in cell death. The mean expression level of p13S15A-GFP was similar to the wild-type.

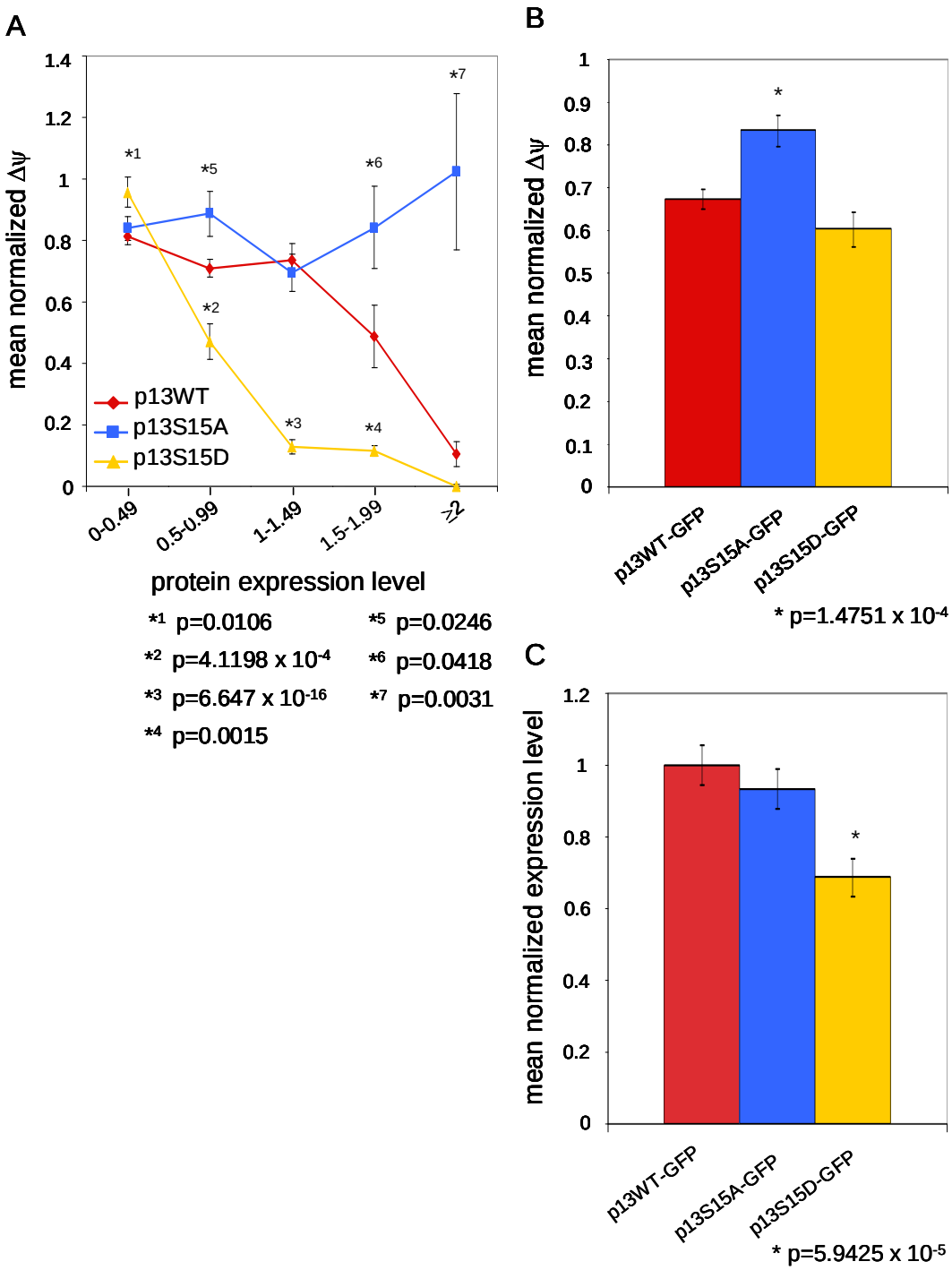

Figure 15: Δψ in cells expressing p13, p13S15A, and p13S15D. Panel A shows TMRM fluorescence plotted against p13 expression ranges, normalized as indicated in Materials and Methods. The data were obtained from the analysis of 244 p13WT-GFP, 184 p13S15A, and 143 p13S15D-GFP cells. The asterisks indicate a significant difference calculated by Student's T test. In p13S15A: $p_{0.5\text{-}0.99}$ = 0.0246; $p_{1.5\text{-}1.99}$ = 0.0418; $p_{\geq 2}$= 0.0031. In p13S15D: $p_{0\text{-}0.49}$ = 0.0106; $p_{0.5\text{-}0.99}$ = 4.1198 x 10^{-4}; $p_{1\text{-}1.49}$ = 6.647 x 10^{-16}; $p_{1.5\text{-}1.99}$ = 0.0015. The graph in Panel B was generated with data pooled from all analyzed cells. The mitochondrial membrane potential is represented as the ratio between the fluorescence intensity (FI) of TMRM in p13WT-, or p13S15A-, or p13S15D-expressing cells and the TMRM mean fluorescence intensity in non-transfected cells. Mean normalized values and standard error bars are reported: $p_{p13S15A}$ = 1.4751 x 10^{-4}. Panel C shows the mean normalized expression levels of p13-GFP, p13S15A-GFP, and p13S15D-GFP, with standard error bars: $p_{p13S15D}$ = 5.9425 x 10^{-5}.

5. DISCUSSION

Previous studies showed that the p13 protein coded by HTLV-1 is specifically targeted to the inner membrane of mitochondria and induces major changes in the morphology of this organelle, causing fragmentation and swelling (Ciminale et al., 1999; D'Agostino et al., 2002). These effects are due to the ability of p13 to increase K^+ permeability of mitochondria (D'Agostino et al., 2002; Silic-Benussi et al., 2009), a property that is dependent on four arginines in the MTS of p13. Recent studies carried out on isolated mitochondria demonstrated that p13 also induces mitochondrial membrane depolarization, influences the activity of the electron transport chain and increases ROS production, and lowers the threshold for PTP opening (Silic-Benussi et al., 2009).

In the present study we measured $\Delta\psi$ in HeLa cells expressing p13-GFP fusion proteins with the potential-dependent probe TMRM. Results demonstrated that p13WT-GFP induces mitochondrial depolarization in a dose-depedent manner. This effect was consistent with previous data obtained using isolated mitochondria and synthetic p13 at increasing concentrations (Silic-Benussi et al., 2009). On the contrary, this effect was not observed with the p13RQ-GFP mutant which carries substitutions of the critical arginine residues in the MTS. These findings are consistent with previous studies which demonstrated that p13RQ is targeted to mitochondria but is unable to induce their fragmentation (D'Agostino et al., 2002).

Interestingly, consistent with previous observations (Ciminale et al., 1999), we observed that cells expressing low to intermediate levels of p13WT-GFP varied in terms of $\Delta\psi$, suggesting that p13 might be necessary but not sufficient to induce mitochondrial depolarization. This observation gave rise to the analysis of the possible role of phosphorylation of p13 in the modulation of its function (see below).

Further analysis of the effect of p13 on $\Delta\psi$ performed in Jurkat T-cells by flow cytometry confirmed the findings made in HeLa cells.

As $\Delta\psi$ is the driving force for mitochondrial Ca^{2+} uptake, we analyzed the intracellular Ca^{2+} concentration in Hela cells cotrasfected with p13, and aequorins targeted to mitochondria, cytosol, and endoplasmic reticulum. This assay is based on the properties of aequorin, a Ca^{2+}-sensitive photoprotein, whose modification with targeting signals for different organelles allows assessement of Ca^{2+} concentration and dynamics within defined cell compartments (Brini et al., 1999; Chiesa et al.,

2001). In these experiments we also tested the mutants p13RQ as well as p13RP and p13RAL, in which the four key arginines were substituted with proline, or with alanine and leucine, respectively; all these mutants maintain the mitochondrial targeting and did not induce mitochondrial fragmentation or depolarization when tested in *in vitro* assays (D'Agostino et al., 2002). Results demonstrated that p13 caused a significative reduction in mitochondrial Ca^{2+} concentration compared to the mock-transfection control. In contrast, the arginine mutants did not affect mitochondrial Ca^{2+} uptake. We found that p13's effects on mitochondrial Ca^{2+} content did not influence cytosolic Ca^{2+} concentration and did not depend on a change in Ca^{2+} release from the ER. The arginine mutants also did not differ substantially from the control in terms of the cytosolic and ER Ca^{2+} content. Taken together, these results demonstrate that p13 specifically reduces mitochondrial Ca^{2+} uptake; the observation that the arginine mutants (p13RQ, p13RAL, p13RP) did not influence mitochondrial Ca^{2+} uptake strongly suggests that this effect is tightly linked to the ability of p13 to induce mitochondrial K^{+} influx and depolarization. It is also possible that p13 affects Ca^{2+} homeostasis through a mechanism involving its ability to promote mitochondrial fragmentation (Ciminale et al., 1999). One might expected that the reduction in mitochondrial Ca^{2+} uptake caused by p13 would have been accompanied by an increase in the cytosolic Ca^{2+} content. However, it must be pointed out that aequorin measures the bulk cytosolic Ca^{2+}, while locally confined increases in Ca^{2+} concentration are not detected. Therefore it is possible that the inefficient mitochondrial Ca^{2+} uptake induced by p13 might cause a local accumulation of Ca^{2+} in the proximity of the plasma membrane or of ER, which would not be evidenced by our assay.

The effects of p13 on Ca^{2+}-homeostasis/signalling might be particularly relevant in the context of T cells, the natural target of HTLV-1 infection, as functional mitochondria are essential for efficient activation through engagement of the T cell receptor complex, allowing the sustained increase of Ca^{2+} necessary for NFAT activation and transcription of its target genes (Hoth et al., 2000; Quintana et al., 2005; Quintana et al., 2006; Quintana et al., 2007). Mitochondria might also play a role during cell-to-cell transmission of HTLV-1 through the "virological synapse", as it was recently demonstrated that mitochondria are redistributed to the contact points between the infected 'donor' cell and the target cell (Majorovits et al., 2008). This possibility would be consistent with the finding that p13 is essential for viral

propagation *in vivo*, documented in a rabbit model (Hiraragi et al., 2006). The alteration in Ca^{2+} homeostasis described in the present study is also consistent with the effect of p13 on Ca^{2+}-dependent CREB phosphorylation reported in a previous study which demonstrated that p13-expressing cells exhibit a marked increase in Ca^{2+}-dependent phosphorylation of the CREB transcription factor (Silic-Benussi et al., 2004). Modulation of CREB phosphorylation by p13 could have important effects on both cell proliferation and HTLV-1 expression in infected cells, given that increased CREB phosphorylation impairs proliferation of cells with mitochondrial defects (Arnould et al., 2002) and that CREB mediates the activation of the HTLV-1 promoter by Tax.

It is interesting to point out that another small HTLV-1 accessory protein, p12, accumulates in the ER and Golgi (Nicot et al., 2005), and interacts with calnexin and calreticulin, two ER-resident proteins that regulate calcium storage (Albrecht et al., 2000; Ding et al., 2001). This interaction results in increased Ca^{2+} release from the ER and decreases the threshold of T-cell activation through NFAT transcriptional activation. These activities of p12 may explain why the protein is required for optimal viral infectivity in quiescent primary cells (Albrecht et al., 2000). Thus, HTLV-1 expresses proteins that impinge on two major organelles controlling the Ca^{2+} signalsome; the possible functional interplay between p12 and p13 represents an attractive subject for future studies of HTLV-1 replication and pathogenesis.

Consistent with these findings, HTLV-1 infection was shown to be associated with an alteration in intracellular Ca^{2+} levels leading to changes in the expression of Ca^{2+}-related genes (Akl et al., 2007).

As previously mentioned, the effect of p13 on $\Delta\psi$ in living cells is heterogeneous, suggesting that additional factors might be critical for the final effect of p13 on mitochondrial function. We hypothesized that p13 function might be regulated by phosphorylation, as *in silico* analysis of p13's amino acid sequence revealed several potential phosphorylation sites (Figure 8). We focused on serine 15, because it was identified as a PKC target site by several prediction programs, and because it is located in the proximity of the critical α-helical domain of p13, essential for its function.

In vitro phosphorylation assays carried out using synthetic peptides spanning residues 9-22, $p13_{[9-22]}$ (RVWTESSFRIPSLR) and $p13S15A_{[9-22]}$ (RVWTESAFRIPSLR), and purified PKC demonstrated that $p13_{[9-22]}$ is markedly

phosphorylated compared to the negative control p13S15A$_{[9-22]}$, which showed a 3-fold reduction in phosphate incorporation compared to the wild-type peptide, suggesting that S15 might be a major PKC target site. The residual phosphorylation of p13S15A might be due to the presence of three other possible phosphorylation sites (T12, S14, and S20). S14 and S20 were predicted to be PKC target sites by NetphosK, and by PROSITE, Scansite and GPS 2.1 software (Xue et al., 2008), respectively.

The PKC family includes several isoforms. Classical or conventional PKCs (α, βI, βII, γ) are Ca^{2+}-dependent and are activated by diacylglycerol (DAG) and phosphatydylserine (PS); novel PKCs (σ, δ, ε, η, θ) are Ca^{2+}-independent and regulated by DAG and PS; atypical PKCs (ζ, λ) are Ca^{2+}-independent and do not require DAG for activation, although PS can regulate their activity. PKCs are involved in cell proliferation, differentiation, and apoptosis, and show different tissue distributions, subcellular localization, modes of activation and substrate specificities. For example, PKCθ, predominantly expressed in T-lymphocytes, is recruited to the immunological synapse during the stimulation of the T-cell recptor (TCR) and is required for T-cell activation (Hayashi and Altman, 2007).

In vitro assays carried out using synthetic p13 protein and cytosolic and mitochondrial extracts prepared from Jurkat T-cells showed that p13 is a good substarte for one or mere protein kinases expressed in these cells. p13WT$_{[9-22]}$ was also readily phosphorylated by the extracts, while the S15A mutant was a much poorer substrate. These studies confirmed S15 to be a major kinase target site in the context of the 9-22 peptide, while T12, S14, and S20 contribute approximately 50% of the peptide's phosphorylation. Furthermore, preliminary data obtained with a PKC inhibitor demonstrated that S15 is specifically phosphorylated by PKC in the mitochondrial lysate (data not shown). Taken together, these studies could help in identifying the kinase responsible for p13 phosphorylation in different intracellular compartments. Considering that in living cells p13 mainly localizes in the inner membrane of mitochondria, its regulation by phosphorylation might result from the activity of a PKC that has the ability to translocate to mitochondria.

In order to analyze the functional effects of the phosphorylation of p13 in S15, we produced the phosphomimetic (p13S15D) and the phosphoablative (p13S15A) mutants by site-specific mutagenesis and analyzed their properties. We found that the aspartic acid mutant induces a more dramatic degree of mitochondrial fragmentation

compared to wild-type p13 and the alanine mutant. Furthermore, analysis of the colocalization indexes with the mitochondrial marker Hsp60, showed that p13S15D mutant accumulates very efficiently in the mitochondrial compartment, but also localizes in the cytoplasm and nucleus, possibly due to the marked disruption of the mitochondrial network. These effects are consistent with the finding that p13S15D induced a marked mitochondrial depolarization in living cells. Interestingly, the phosphoablative mutant fragmented mitochondria but did not depolarize them. These findings let us to conclude that phosphorylation on S15 may modulate the protein's impact on mitochondrial function.

Interestingly, p13 was predicted to be phosphorylated on S15 by PKCδ and PKCθ using GPS 2.1 software (data not shown). PKCδ was found to translocate to mitochondria upon oxidative stress, and was associated with the loss of $\Delta\psi$ and the release of cytochrome c (Majumder et al., 2001). As p13 induces ROS production in isolated mitochondria (Silic-Benussi et al., 2009) and in living cells (Silic-Benussi et al., manuscript submitted), the hypothetical activation of PKCδ mediated by p13 through ROS production might in turn regulate p13's effects by phosphorylation of S15. PKCθ was also demonstrated to translocate to mitochondria after T-cell activation and is essential for activation-induced ROS production (Kaminski et al., 2007). Another PKC isoform that is able to translocate to mitochondria is PKCε, which interacts with several mitochondrial proteins (Baines et al., 2003) and activates mitoK_{ATP} channels (Jaburek et al., 2006) which promote cardioprotection during ischemic preconditioning.

It is noteworthy that ATLL cells exhibit an altered expression of PKC, compared to control T-lymphocytes obtained from healty donors (Hidaka et al., 1992), and that specific PKC isoforms are involved in activation of the HTLV-1 LTR (Chamias et al., 2009). Furthermore, Tax is able to bind PKCα, PKCδ, and PKCη and to increase PKC translocation into membranes (Lindholm et al., 1996). Therefore, the pattern of phosphorylation of p13 may be influenced by the presence of Tax.

Two-dimensional analysis of lysates of Jurkat T-cells transiently transfected with p13 showed that the protein migrated as two main spots, one at pI 9 and the other at a pI comprised between 4 and 5, which might represent a hyperphosphorylated form of p13. The *in silico* analysis of p13's amino acid sequence revealed several sites that might be targets of other kinases (Figure 8). Of these, T78 is predicted to be a putative target site for p38MAPK, GSK3, and cdk5 by several prediction programs.

T78 might be a key site, as it is located in the C-terminal portion of the protein, which contains several PXXP motif that could mediate its binding to proteins containing SH3 domains. Future studies will thus be aimed at characterizing additional phosphoacceptor sites of p13.

Current studies are aimed at studying p13 phosphorylation by mass spectrometry and metabolic labelling with ^{32}P ortho-phosphate. Furthermore, our efforts will be aimed at the identification of the pathway involved in p13 phosphorylation by testing different and specific kinase activators and inhibitors in *in vitro* assays, and testing other functional effects of S15 phophorylation in isolated mitochondria and in living cells.

RINGRAZIAMENTI

Desidero ringraziare tutte le persone che mi hanno accompagnato in questo percorso a che hanno in vario modo contribuito a questo lavoro di tesi.

Prima di tutto, un grandissimo ringraziamento va a Vincenzo e a Donna, per avermi insegnato un sacco di cose, avermi dato la possibilità di lavorare qui da loro, in un ambiente stimolante e "familiare", per il costante aiuto e la disponibilità, e per avermi sempre sostenuto.

Ringrazio tutte le colleghe di laboratorio Katia, Francesca, Ilaria, Micol, Mariangela, e anche Enrica e Paola, che hanno preso altre strade, e i dottorandi e colleghi del Dipartimento, con cui ho condiviso le mie giornate e la mia quotidianità.

Un particolare e speciale ringraziamento va ad Andrea Venerando e Oriano Marin, per la collaborazione entusiasta, attiva e produttiva a questo progetto, per la presenza, l'aiuto e disponibilità che mi hanno sempre dimostrato.

Ringrazio Paola Aguiari, Paolo Pinton e Rosario Rizzuto per la proficua collaborazione sul progetto calcio.

Ringrazio Barbara Seliger, che mi ha ospitato nel suo laboratorio ad Halle, dandomi la possibilità di imparare ed approfondire la tecnica 2D, e ringrazio Rudi Lichtenfels e Christian Recktenwald, gli "insegnanti" che si sono presi cura di me durante il mese trascorso lì.

Ringrazio il Prof. Chieco-Bianchi per la disponibilità e l'attenta supervisione.

Ringrazio Daniela Saggioro per i preziosi consigli.

Un grazie agli informatici Renzo e Pierantonio, il cui aiuto e supporto è sempre fondamentale.

Ringrazio i lab meeting di Bernardi (gli organizzatori Paolo Bernardi, Andrea Rasola e Luca Scorrano, e tutti i partecipanti) che mi hanno permesso di fare "palestra" per presentazioni e congressi.

Infine, un caro ringraziamento alla mia famiglia e un grazie speciale a Nabil.

6. REFERENCES

Adachi, Y., Nosaka, T., and Hatanaka, M. (1990). Protein kinase inhibitor H-7 blocks accumulation of unspliced mRNA of human T-cell leukemia virus type I (HTLV-I). Biochemical and biophysical research communications *169*, 469-475.

Akl, H., Badran, B.M., Zein, N.E., Bex, F., Sotiriou, C., Willard-Gallo, K.E., Burny, A., and Martiat, P. (2007). HTLV-I infection of WE17/10 CD4+ cell line leads to progressive alteration of Ca2+ influx that eventually results in loss of CD7 expression and activation of an antiapoptotic pathway involving AKT and BAD which paves the way for malignant transformation. Leukemia *21*, 788-796.

Albrecht, B., Collins, N.D., Burniston, M.T., Nisbet, J.W., Ratner, L., Green, P.L., and Lairmore, M.D. (2000). Human T-lymphotropic virus type 1 open reading frame I p12(I) is required for efficient viral infectivity in primary lymphocytes. Journal of virology *74*, 9828-9835.

Albrecht, B., D'Souza, C.D., Ding, W., Tridandapani, S., Coggeshall, K.M., and Lairmore, M.D. (2002). Activation of nuclear factor of activated T cells by human T-lymphotropic virus type 1 accessory protein p12(I). Journal of virology *76*, 3493-3501.

Araujo, A., and Hall, W.W. (2004). Human T-lymphotropic virus type II and neurological disease. Annals of neurology *56*, 10-19.

Arnold, J., Yamamoto, B., Li, M., Phipps, A.J., Younis, I., Lairmore, M.D., and Green, P.L. (2006). Enhancement of infectivity and persistence in vivo by HBZ, a natural antisense coded protein of HTLV-1. Blood *107*, 3976-3982.

Arnold, J., Zimmerman, B., Li, M., Lairmore, M.D., and Green, P.L. (2008). Human T-cell leukemia virus type-1 antisense-encoded gene, Hbz, promotes T-lymphocyte proliferation. Blood *112*, 3788-3797.

Arnould, T., Vankoningsloo, S., Renard, P., Houbion, A., Ninane, N., Demazy, C., Remacle, J., and Raes, M. (2002). CREB activation induced by mitochondrial dysfunction is a new signaling pathway that impairs cell proliferation. Embo J *21*, 53-63.

Awasthi, S., Sharma, A., Wong, K., Zhang, J., Matlock, E.F., Rogers, L., Motloch, P., Takemoto, S., Taguchi, H., Cole, M.D., *et al.* (2005). A human T-cell lymphotropic virus type 1 enhancer of Myc transforming potential stabilizes Myc-TIP60 transcriptional interactions. Molecular and cellular biology *25*, 6178-6198.

Baines, C.P., Song, C.X., Zheng, Y.T., Wang, G.W., Zhang, J., Wang, O.L., Guo, Y., Bolli, R., Cardwell, E.M., and Ping, P. (2003). Protein kinase Cepsilon interacts with and inhibits the permeability transition pore in cardiac mitochondria. Circulation research *92*, 873-880.

Bairoch, A., Bucher, P., and Hofmann, K. (1997). The PROSITE database, its status in 1997. Nucleic acids research *25*, 217-221.

Bakker, A., Li, X., Ruland, C.T., Stephens, D.W., Black, A.C., and Rosenblatt, J.D. (1996). Human T-cell leukemia virus type 2 Rex inhibits pre-mRNA splicing in vitro at an early stage of spliceosome formation. Journal of virology *70*, 5511-5518.

Banerjee, P., Feuer, G., and Barker, E. (2007). Human T-cell leukemia virus type 1 (HTLV-1) p12I down-modulates ICAM-1 and -2 and reduces adherence of natural killer cells, thereby protecting HTLV-1-infected primary CD4+ T cells from autologous natural killer cell-mediated cytotoxicity despite the reduction of major histocompatibility complex class I molecules on infected cells. Journal of virology *81*, 9707-9717.

Bangham, C.R. (2003). The immune control and cell-to-cell spread of human T-lymphotropic virus type 1. The Journal of general virology *84*, 3177-3189.

Barmak, K., Harhaj, E., Grant, C., Alefantis, T., and Wigdahl, B. (2003). Human T cell leukemia virus type I-induced disease: pathways to cancer and neurodegeneration. Virology *308*, 1-12.

Barnard, A.L., Igakura, T., Tanaka, Y., Taylor, G.P., and Bangham, C.R. (2005). Engagement of specific T-cell surface molecules regulates cytoskeletal polarization in HTLV-1-infected lymphocytes. Blood *106*, 988-995.

Bartoe, J.T., Albrecht, B., Collins, N.D., Robek, M.D., Ratner, L., Green, P.L., and Lairmore, M.D. (2000). Functional role of pX open reading frame II of human T-lymphotropic virus type 1 in maintenance of viral loads in vivo. Journal of virology *74*, 1094-1100.

Basbous, J., Arpin, C., Gaudray, G., Piechaczyk, M., Devaux, C., and Mesnard, J.M. (2003). The HBZ factor of human T-cell leukemia virus type I dimerizes with transcription factors JunB and c-Jun and modulates their transcriptional activity. The Journal of biological chemistry *278*, 43620-43627.

Bergqvist, A., Sundstrom, S., Dimberg, L.Y., Gylfe, E., and Masucci, M.G. (2003). The hepatitis C virus core protein modulates T cell responses by inducing spontaneous and altering T-cell receptor-triggered Ca2+ oscillations. The Journal of biological chemistry *278*, 18877-18883.

Blom, N., Gammeltoft, S., and Brunak, S. (1999). Sequence and structure-based prediction of eukaryotic protein phosphorylation sites. Journal of molecular biology *294*, 1351-1362.

Blom, N., Sicheritz-Ponten, T., Gupta, R., Gammeltoft, S., and Brunak, S. (2004). Prediction of post-translational glycosylation and phosphorylation of proteins from the amino acid sequence. Proteomics *4*, 1633-1649.

Blot, V., Delamarre, L., Perugi, F., Pham, D., Benichou, S., Benarous, R., Hanada, T., Chishti, A.H., Dokhelar, M.C., and Pique, C. (2004). Human Dlg protein binds to the envelope glycoproteins of human T-cell leukemia virus type 1 and regulates envelope mediated cell-cell fusion in T lymphocytes. Journal of cell science *117*, 3983-3993.

Bogerd, H., and Greene, W.C. (1993). Dominant negative mutants of human T-cell leukemia virus type I Rex and human immunodeficiency virus type 1 Rev fail to multimerize in vivo. Journal of virology *67*, 2496-2502.

Bogerd, H.P., Echarri, A., Ross, T.M., and Cullen, B.R. (1998). Inhibition of human immunodeficiency virus Rev and human T-cell leukemia virus Rex function, but not Mason-Pfizer monkey virus constitutive transport element activity, by a mutant human nucleoporin targeted to Crm1. Journal of virology *72*, 8627-8635.

Bogerd, H.P., Fridell, R.A., Madore, S., and Cullen, B.R. (1995). Identification of a novel cellular cofactor for the Rev/Rex class of retroviral regulatory proteins. Cell *82*, 485-494.

Boya, P., Pauleau, A.L., Poncet, D., Gonzalez-Polo, R.A., Zamzami, N., and Kroemer, G. (2004). Viral proteins targeting mitochondria: controlling cell death. Biochimica et biophysica acta *1659*, 178-189.

Brini, M., Pinton, P., Pozzan, T., and Rizzuto, R. (1999). Targeted recombinant aequorins: tools for monitoring [Ca2+] in the various compartments of a living cell. Microscopy research and technique *46*, 380-389.

Cereghetti, G.M., and Scorrano, L. (2006). The many shapes of mitochondrial death. Oncogene *25*, 4717-4724.

Chami, M., Ferrari, D., Nicotera, P., Paterlini-Brechot, P., and Rizzuto, R. (2003). Caspase-dependent alterations of Ca2+ signaling in the induction of apoptosis by hepatitis B virus X protein. The Journal of biological chemistry *278*, 31745-31755.

Chami, M., Oules, B., and Paterlini-Brechot, P. (2006). Cytobiological consequences of calcium-signaling alterations induced by human viral proteins. Biochimica et biophysica acta *1763*, 1344-1362.

Chamias, R., Huleihel, M., and Aboud, M. (2009). The mechanism of HTLV-1 LTR activation by TPA varies in different human T-cell lines: Role of specific PKC isoforms. Leukemia research.

Chiesa, A., Rapizzi, E., Tosello, V., Pinton, P., de Virgilio, M., Fogarty, K.E., and Rizzuto, R. (2001). Recombinant aequorin and green fluorescent protein as valuable tools in the study of cell signalling. The Biochemical journal *355*, 1-12.

Ciminale, V., Pavlakis, G.N., Derse, D., Cunningham, C.P., and Felber, B.K. (1992). Complex splicing in the human T-cell leukemia virus (HTLV) family of retroviruses: novel mRNAs and proteins produced by HTLV type I. Journal of virology *66*, 1737-1745.

Ciminale, V., Zotti, L., D'Agostino, D.M., Ferro, T., Casareto, L., Franchini, G., Bernardi, P., and Chieco-Bianchi, L. (1999). Mitochondrial targeting of the p13II protein coded by the x-II ORF of human T-cell leukemia/lymphotropic virus type I (HTLV-I). Oncogene *18*, 4505-4514.

Collins, N.D., Newbound, G.C., Ratner, L., and Lairmore, M.D. (1996). In vitro CD4+ lymphocyte transformation and infection in a rabbit model with a molecular clone of human T-cell lymphotrophic virus type 1. Journal of virology *70*, 7241-7246.

D'Agostino, D.M., Bernardi, P., Chieco-Bianchi, L., and Ciminale, V. (2005a). Mitochondria as functional targets of proteins coded by human tumor viruses. Adv Cancer Res *94*, 87-142.

D'Agostino, D.M., Ciminale, V., Zotti, L., Rosato, A., and Chieco-Bianchi, L. (1997). The human T-cell lymphotropic virus type 1 Tof protein contains a bipartite nuclear localization signal that is able to functionally replace the amino-terminal domain of Rex. Journal of virology *71*, 75-83.

D'Agostino, D.M., Ranzato, L., Arrigoni, G., Cavallari, I., Belleudi, F., Torrisi, M.R., Silic-Benussi, M., Ferro, T., Petronilli, V., Marin, O., *et al.* (2002). Mitochondrial alterations induced by the p13II protein of human T-cell leukemia virus type 1. Critical role of arginine residues. The Journal of biological chemistry *277*, 34424-34433.

D'Agostino, D.M., Silic-Benussi, M., Hiraragi, H., Lairmore, M.D., and Ciminale, V. (2005b). The human T-cell leukemia virus type 1 p13II protein: effects on mitochondrial function and cell growth. Cell Death Differ *12 Suppl 1*, 905-915.

D'Agostino, D.M., Zotti, L., Ferro, T., Cavallori, I., Silic-Benussi, M., Chieco-Bianchi, L., and Ciminale, V. (2001). Expression and functional properties of proteins encoded in the x-II ORF of HTLV-I. Virus research *78*, 35-43.

D'Agostino, D.M., Zotti, L., Ferro, T., Franchini, G., Chieco-Bianchi, L., and Ciminale, V. (2000). The p13II protein of HTLV type 1: comparison with mitochondrial proteins coded by other human viruses. AIDS Res Hum Retroviruses *16*, 1765-1770.

Datta, A., Sinha-Datta, U., Dhillon, N.K., Buch, S., and Nicot, C. (2006). The HTLV-I p30 interferes with TLR4 signaling and modulates the release of pro- and anti-inflammatory cytokines from human macrophages. The Journal of biological chemistry *281*, 23414-23424.

Derse, D., Mikovits, J., and Ruscetti, F. (1997). X-I and X-II open reading frames of HTLV-I are not required for virus replication or for immortalization of primary T-cells in vitro. Virology *237*, 123-128.

Dietel, M., Herzig, I., Reymann, A., Brandt, I., Schaefer, B., Bunge, A., Heidebrecht, H.J., and Seidel, A. (1994). Secondary combined resistance to the multidrug-resistance-reversing activity of cyclosporin A in the cell line F4-6RADR-CsA. Journal of cancer research and clinical oncology *120*, 263-271.

Ding, W., Albrecht, B., Kelley, R.E., Muthusamy, N., Kim, S.J., Altschuld, R.A., and Lairmore, M.D. (2002). Human T-cell lymphotropic virus type 1 p12(I) expression increases cytoplasmic calcium to enhance the activation of nuclear factor of activated T cells. Journal of virology *76*, 10374-10382.

Ding, W., Albrecht, B., Luo, R., Zhang, W., Stanley, J.R., Newbound, G.C., and Lairmore, M.D. (2001). Endoplasmic reticulum and cis-Golgi localization of human T-lymphotropic

virus type 1 p12(I): association with calreticulin and calnexin. Journal of virology *75*, 7672-7682.

Durkin, S.S., Ward, M.D., Fryrear, K.A., and Semmes, O.J. (2006). Site-specific phosphorylation differentiates active from inactive forms of the human T-cell leukemia virus type 1 Tax oncoprotein. The Journal of biological chemistry *281*, 31705-31712.

Falquet, L., Pagni, M., Bucher, P., Hulo, N., Sigrist, C.J., Hofmann, K., and Bairoch, A. (2002). The PROSITE database, its status in 2002. Nucleic acids research *30*, 235-238.

Felber, B.K., Paskalis, H., Kleinman-Ewing, C., Wong-Staal, F., and Pavlakis, G.N. (1985). The pX protein of HTLV-I is a transcriptional activator of its long terminal repeats. Science (New York, NY *229*, 675-679.

Feske, S. (2007). Calcium signalling in lymphocyte activation and disease. Nature reviews *7*, 690-702.

Feuer, G., and Green, P.L. (2005). Comparative biology of human T-cell lymphotropic virus type 1 (HTLV-1) and HTLV-2. Oncogene *24*, 5996-6004.

Fields, G.B., and Noble, R.L. (1990). Solid phase peptide synthesis utilizing 9-fluorenylmethoxycarbonyl amino acids. International journal of peptide and protein research *35*, 161-214.

Gatza, M.L., Watt, J.C., and Marriott, S.J. (2003). Cellular transformation by the HTLV-I Tax protein, a jack-of-all-trades. Oncogene *22*, 5141-5149.

Gaudray, G., Gachon, F., Basbous, J., Biard-Piechaczyk, M., Devaux, C., and Mesnard, J.M. (2002). The complementary strand of the human T-cell leukemia virus type 1 RNA genome encodes a bZIP transcription factor that down-regulates viral transcription. Journal of virology *76*, 12813-12822.

Gessain, A., Barin, F., Vernant, J.C., Gout, O., Maurs, L., Calender, A., and de The, G. (1985). Antibodies to human T-lymphotropic virus type-I in patients with tropical spastic paraparesis. Lancet *2*, 407-410.

Ghez, D., Lepelletier, Y., Lambert, S., Fourneau, J.M., Blot, V., Janvier, S., Arnulf, B., van Endert, P.M., Heveker, N., Pique, C., *et al.* (2006). Neuropilin-1 is involved in human T-cell lymphotropic virus type 1 entry. Journal of virology *80*, 6844-6854.

Gibbs, J.S., Malide, D., Hornung, F., Bennink, J.R., and Yewdell, J.W. (2003). The influenza A virus PB1-F2 protein targets the inner mitochondrial membrane via a predicted basic amphipathic helix that disrupts mitochondrial function. Journal of virology *77*, 7214-7224.

Gonzalez, M.E., and Carrasco, L. (2003). Viroporins. FEBS letters *552*, 28-34.

Green, P.L., and Chen, I.S.Y. (2001). Human T-cell leukemia virus types 1 and 2. In Fields Virology, D.M.a.H. Knipe, P.M., ed. (Philadelphia, Lippincott Williams and Wilkins), pp. 1941-1970.

Griffin, S.D., Beales, L.P., Clarke, D.S., Worsfold, O., Evans, S.D., Jaeger, J., Harris, M.P., and Rowlands, D.J. (2003). The p7 protein of hepatitis C virus forms an ion channel that is blocked by the antiviral drug, Amantadine. FEBS letters *535*, 34-38.

Gunter, T.E., Yule, D.I., Gunter, K.K., Eliseev, R.A., and Salter, J.D. (2004). Calcium and mitochondria. FEBS letters *567*, 96-102.

Haqshenas, G., Mackenzie, J.M., Dong, X., and Gowans, E.J. (2007). Hepatitis C virus p7 protein is localized in the endoplasmic reticulum when it is encoded by a replication-competent genome. The Journal of general virology *88*, 134-142.

Hayashi, K., and Altman, A. (2007). Protein kinase C theta (PKCtheta): a key player in T cell life and death. Pharmacol Res *55*, 537-544.

Heger, P., Rosorius, O., Hauber, J., and Stauber, R.H. (1999). Titration of cellular export factors, but not heteromultimerization, is the molecular mechanism of trans-dominant HTLV-1 rex mutants. Oncogene *18*, 4080-4090.

Hidaka, M., Nakakuma, H., Kawaguchi, T., Nagakura, S., Horikawa, K., Okuno, Y., Kagimoto, T., and Takatsuki, K. (1992). Altered expression of protein kinase C in adult T-cell leukemia cells. International journal of hematology *56*, 135-141.

Hinuma, Y., Nagata, K., Hanaoka, M., Nakai, M., Matsumoto, T., Kinoshita, K.I., Shirakawa, S., and Miyoshi, I. (1981). Adult T-cell leukemia: antigen in an ATL cell line and detection of antibodies to the antigen in human sera. Proceedings of the National Academy of Sciences of the United States of America *78*, 6476-6480.

Hiraragi, H., Kim, S.J., Phipps, A.J., Silic-Benussi, M., Ciminale, V., Ratner, L., Green, P.L., and Lairmore, M.D. (2006). Human T-lymphotropic virus type 1 mitochondrion-localizing protein p13(II) is required for viral infectivity in vivo. Journal of virology *80*, 3469-3476.

Hiraragi, H., Michael, B., Nair, A., Silic-Benussi, M., Ciminale, V., and Lairmore, M. (2005). Human T-lymphotropic virus type 1 mitochondrion-localizing protein p13II sensitizes Jurkat T cells to Ras-mediated apoptosis. Journal of virology *79*, 9449-9457.

Hivin, P., Frederic, M., Arpin-Andre, C., Basbous, J., Gay, B., Thebault, S., and Mesnard, J.M. (2005). Nuclear localization of HTLV-I bZIP factor (HBZ) is mediated by three distinct motifs. Journal of cell science *118*, 1355-1362.

Hope, T.J., Bond, B.L., McDonald, D., Klein, N.P., and Parslow, T.G. (1991). Effector domains of human immunodeficiency virus type 1 Rev and human T-cell leukemia virus type I Rex are functionally interchangeable and share an essential peptide motif. Journal of virology *65*, 6001-6007.

Hoth, M., Button, D.C., and Lewis, R.S. (2000). Mitochondrial control of calcium-channel gating: a mechanism for sustained signaling and transcriptional activation in T lymphocytes. Proceedings of the National Academy of Sciences of the United States of America *97*, 10607-10612.

Igakura, T., Stinchcombe, J.C., Goon, P.K., Taylor, G.P., Weber, J.N., Griffiths, G.M., Tanaka, Y., Osame, M., and Bangham, C.R. (2003). Spread of HTLV-I between lymphocytes by virus-induced polarization of the cytoskeleton. Science (New York, NY *299*, 1713-1716.

Iwasaki, Y. (1990). Pathology of chronic myelopathy associated with HTLV-I infection (HAM/TSP). Journal of the neurological sciences *96*, 103-123.

Jaburek, M., Costa, A.D., Burton, J.R., Costa, C.L., and Garlid, K.D. (2006). Mitochondrial PKC epsilon and mitochondrial ATP-sensitive K+ channel copurify and coreconstitute to form a functioning signaling module in proteoliposomes. Circulation research *99*, 878-883.

Jacotot, E., Ravagnan, L., Loeffler, M., Ferri, K.F., Vieira, H.L., Zamzami, N., Costantini, P., Druillennec, S., Hoebeke, J., Briand, J.P., *et al.* (2000). The HIV-1 viral protein R induces apoptosis via a direct effect on the mitochondrial permeability transition pore. The Journal of experimental medicine *191*, 33-46.

Johnson, J.M., Nicot, C., Fullen, J., Ciminale, V., Casareto, L., Mulloy, J.C., Jacobson, S., and Franchini, G. (2001). Free major histocompatibility complex class I heavy chain is preferentially targeted for degradation by human T-cell leukemia/lymphotropic virus type 1 p12(I) protein. Journal of virology *75*, 6086-6094.

Kaminski, M., Kiessling, M., Suss, D., Krammer, P.H., and Gulow, K. (2007). Novel role for mitochondria: protein kinase Ctheta-dependent oxidative signaling organelles in activation-induced T-cell death. Molecular and cellular biology *27*, 3625-3639.

Karube, K., Ohshima, K., Tsuchiya, T., Yamaguchi, T., Kawano, R., Suzumiya, J., Utsunomiya, A., Harada, M., and Kikuchi, M. (2004). Expression of FoxP3, a key molecule in CD4CD25 regulatory T cells, in adult T-cell leukaemia/lymphoma cells. British journal of haematology *126*, 81-84.

Kashanchi, F., and Brady, J.N. (2005). Transcriptional and post-transcriptional gene regulation of HTLV-1. Oncogene *24*, 5938-5951.

Kawano, F., Yamaguchi, K., Nishimura, H., Tsuda, H., and Takatsuki, K. (1985). Variation in the clinical courses of adult T-cell leukemia. Cancer *55*, 851-856.

Kennelly, P.J., and Krebs, E.G. (1991). Consensus sequences as substrate specificity determinants for protein kinases and protein phosphatases. The Journal of biological chemistry *266*, 15555-15558.

Kesic, M., Doueiri, R., Ward, M., Semmes, O.J., and Green, P.L. (2009). Phosphorylation regulates human T-cell leukemia virus type 1 Rex function. Retrovirology *6*, 105.

Kim, S.J., Ding, W., Albrecht, B., Green, P.L., and Lairmore, M.D. (2003). A conserved calcineurin-binding motif in human T lymphotropic virus type 1 p12I functions to modulate nuclear factor of activated T cell activation. The Journal of biological chemistry *278*, 15550-15557.

Kirichok, Y., Krapivinsky, G., and Clapham, D.E. (2004). The mitochondrial calcium uniporter is a highly selective ion channel. Nature *427*, 360-364.

Koralnik, I.J., Fullen, J., and Franchini, G. (1993). The p12I, p13II, and p30II proteins encoded by human T-cell leukemia/lymphotropic virus type I open reading frames I and II are localized in three different cellular compartments. Journal of virology *67*, 2360-2366.

Koralnik, I.J., Gessain, A., Klotman, M.E., Lo Monico, A., Berneman, Z.N., and Franchini, G. (1992). Protein isoforms encoded by the pX region of human T-cell leukemia/lymphotropic virus type I. Proceedings of the National Academy of Sciences of the United States of America *89*, 8813-8817.

Kroemer, G., Galluzzi, L., and Brenner, C. (2007). Mitochondrial membrane permeabilization in cell death. Physiological reviews *87*, 99-163.

Kuhlmann, A.S., Villaudy, J., Gazzolo, L., Castellazzi, M., Mesnard, J.M., and Duc Dodon, M. (2007). HTLV-1 HBZ cooperates with JunD to enhance transcription of the human telomerase reverse transcriptase gene (hTERT). Retrovirology *4*, 92.

Lairmore, M.D., and Franchini, G. (2007). Human T-cell leukemia virus types 1 and 2. Howley DMKaPM, ed Fields Virology, Fifth Edition, Philadelphia: Lippincott Williams and Wilkins *Vol 2.*, 2071-2106.

Larocca, D., Chao, L.A., Seto, M.H., and Brunck, T.K. (1989). Human T-cell leukemia virus minus strand transcription in infected T-cells. Biochemical and biophysical research communications *163*, 1006-1013.

Le Blanc, I., Grange, M.P., Delamarre, L., Rosenberg, A.R., Blot, V., Pique, C., and Dokhelar, M.C. (2001). HTLV-1 structural proteins. Virus research *78*, 5-16.

Lemasson, I., Lewis, M.R., Polakowski, N., Hivin, P., Cavanagh, M.H., Thebault, S., Barbeau, B., Nyborg, J.K., and Mesnard, J.M. (2007). Human T-cell leukemia virus type 1 (HTLV-1) bZIP protein interacts with the cellular transcription factor CREB to inhibit HTLV-1 transcription. Journal of virology *81*, 1543-1553.

Lewis, R.S. (2007). The molecular choreography of a store-operated calcium channel. Nature *446*, 284-287.

Li, J., Li, H., and Tsai, M.D. (2003). Direct binding of the N-terminus of HTLV-1 tax oncoprotein to cyclin-dependent kinase 4 is a dominant path to stimulate the kinase activity. Biochemistry *42*, 6921-6928.

Lindholm, P.F., Tamami, M., Makowski, J., and Brady, J.N. (1996). Human T-cell lymphotropic virus type 1 Tax1 activation of NF-kappa B: involvement of the protein kinase C pathway. Journal of virology *70*, 2525-2532.

Liu, B., Hong, S., Tang, Z., Yu, H., and Giam, C.Z. (2005). HTLV-I Tax directly binds the Cdc20-associated anaphase-promoting complex and activates it ahead of schedule. Proceedings of the National Academy of Sciences of the United States of America *102*, 63-68.

Mahieux, R., and Gessain, A. (2009). The human HTLV-3 and HTLV-4 retroviruses: new members of the HTLV family. Pathologie-biologie *57*, 161-166.

Majorovits, E., Nejmeddine, M., Tanaka, Y., Taylor, G.P., Fuller, S.D., and Bangham, C.R. (2008). Human T-lymphotropic virus-1 visualized at the virological synapse by electron tomography. PloS one *3*, e2251.

Majumder, P.K., Mishra, N.C., Sun, X., Bharti, A., Kharbanda, S., Saxena, S., and Kufe, D. (2001). Targeting of protein kinase C delta to mitochondria in the oxidative stress response. Cell Growth Differ *12*, 465-470.

Manel, N., Battini, J.L., Taylor, N., and Sitbon, M. (2005). HTLV-1 tropism and envelope receptor. Oncogene *24*, 6016-6025.

Manel, N., Kim, F.J., Kinet, S., Taylor, N., Sitbon, M., and Battini, J.L. (2003). The ubiquitous glucose transporter GLUT-1 is a receptor for HTLV. Cell *115*, 449-459.

Manninen, A., and Saksela, K. (2002). HIV-1 Nef interacts with inositol trisphosphate receptor to activate calcium signaling in T cells. The Journal of experimental medicine *195*, 1023-1032.

Matsumoto, J., Ohshima, T., Isono, O., and Shimotohno, K. (2005). HTLV-1 HBZ suppresses AP-1 activity by impairing both the DNA-binding ability and the stability of c-Jun protein. Oncogene *24*, 1001-1010.

Matsuoka, M., and Green, P.L. (2009). The HBZ gene, a key player in HTLV-1 pathogenesis. Retrovirology *6*, 71.

Michael, B., Nair, A.M., Hiraragi, H., Shen, L., Feuer, G., Boris-Lawrie, K., and Lairmore, M.D. (2004). Human T lymphotropic virus type-1 p30II alters cellular gene expression to selectively enhance signaling pathways that activate T lymphocytes. Retrovirology *1*, 39.

Mitzner, D., Dudek, S.E., Studtrucker, N., Anhlan, D., Mazur, I., Wissing, J., Jansch, L., Wixler, L., Bruns, K., Sharma, A., *et al.* (2009). Phosphorylation of the influenza A virus protein PB1-F2 by PKC is crucial for apoptosis promoting functions in monocytes. Cellular microbiology *11*, 1502-1516.

Miyazaki, M., Yasunaga, J., Taniguchi, Y., Tamiya, S., Nakahata, T., and Matsuoka, M. (2007). Preferential selection of human T-cell leukemia virus type 1 provirus lacking the 5' long terminal repeat during oncogenesis. Journal of virology *81*, 5714-5723.

Mochizuki, M., Ono, A., Ikeda, E., Hikita, N., Watanabe, T., Yamaguchi, K., Sagawa, K., and Ito, K. (1996). HTLV-I uveitis. J Acquir Immune Defic Syndr Hum Retrovirol *13 Suppl 1*, S50-56.

Mulloy, J.C., Crownley, R.W., Fullen, J., Leonard, W.J., and Franchini, G. (1996). The human T-cell leukemia/lymphotropic virus type 1 p12I proteins bind the interleukin-2 receptor beta and gammac chains and affects their expression on the cell surface. Journal of virology *70*, 3599-3605.

Narayan, M., Younis, I., D'Agostino, D.M., and Green, P.L. (2003). Functional domain structure of human T-cell leukemia virus type 2 rex. Journal of virology *77*, 12829-12840.

Nasmyth, K. (2005). How do so few control so many? Cell *120*, 739-746.

Nejmeddine, M., Barnard, A.L., Tanaka, Y., Taylor, G.P., and Bangham, C.R. (2005). Human T-lymphotropic virus, type 1, tax protein triggers microtubule reorientation in the virological synapse. The Journal of biological chemistry *280*, 29653-29660.

Nejmeddine, M., Negi, V.S., Mukherjee, S., Tanaka, Y., Orth, K., Taylor, G.P., and Bangham, C.R. (2009). HTLV-1-Tax and ICAM-1 act on T-cell signal pathways to polarize the microtubule-organizing center at the virological synapse. Blood *114*, 1016-1025.

Nicot, C., Dundr, M., Johnson, J.M., Fullen, J.R., Alonzo, N., Fukumoto, R., Princler, G.L., Derse, D., Misteli, T., and Franchini, G. (2004). HTLV-1-encoded p30(II) is a post-transcriptional negative regulator of viral replication. Nature medicine.

Nicot, C., Harrod, R.L., Ciminale, V., and Franchini, G. (2005). Human T-cell leukemia/lymphoma virus type 1 nonstructural genes and their functions. Oncogene *24*, 6026-6034.

Nicot, C., Mulloy, J.C., Ferrari, M.G., Johnson, J.M., Fu, K., Fukumoto, R., Trovato, R., Fullen, J., Leonard, W.J., and Franchini, G. (2001). HTLV-1 p12(I) protein enhances STAT5 activation and decreases the interleukin-2 requirement for proliferation of primary human peripheral blood mononuclear cells. Blood *98*, 823-829.

Nishikawa, K., Toker, A., Johannes, F.J., Songyang, Z., and Cantley, L.C. (1997). Determination of the specific substrate sequence motifs of protein kinase C isozymes. The Journal of biological chemistry *272*, 952-960.

Obenauer, J.C., Cantley, L.C., and Yaffe, M.B. (2003). Scansite 2.0: Proteome-wide prediction of cell signaling interactions using short sequence motifs. Nucleic acids research *31*, 3635-3641.

Osame, M. (2002). Pathological mechanisms of human T-cell lymphotropic virus type I-associated myelopathy (HAM/TSP). Journal of neurovirology *8*, 359-364.

Osame, M., Usuku, K., Izumo, S., Ijichi, N., Amitani, H., Igata, A., Matsumoto, M., and Tara, M. (1986). HTLV-I associated myelopathy, a new clinical entity. Lancet *1*, 1031-1032.

Overbaugh, J., and Bangham, C.R. (2001). Selection forces and constraints on retroviral sequence variation. Science (New York, NY *292*, 1106-1109.

Pais-Correia, A.M., Sachse, M., Guadagnini, S., Robbiati, V., Lasserre, R., Gessain, A., Gout, O., Alcover, A., and Thoulouze, M.I. (2010). Biofilm-like extracellular viral assemblies mediate HTLV-1 cell-to-cell transmission at virological synapses. Nature medicine *16*, 83-89.

Pavlovic, D., Neville, D.C., Argaud, O., Blumberg, B., Dwek, R.A., Fischer, W.B., and Zitzmann, N. (2003). The hepatitis C virus p7 protein forms an ion channel that is inhibited by long-alkyl-chain iminosugar derivatives. Proceedings of the National Academy of Sciences of the United States of America *100*, 6104-6108.

Petronilli, V., Miotto, G., Canton, M., Colonna, R., Bernardi, P., and Di Lisa, F. (1998). Imaging the mitochondrial permeability transition pore in intact cells. Biofactors *8*, 263-272.

Pinon, J.D., Klasse, P.J., Jassal, S.R., Welson, S., Weber, J., Brighty, D.W., and Sattentau, Q.J. (2003). Human T-cell leukemia virus type 1 envelope glycoprotein gp46 interacts with cell surface heparan sulfate proteoglycans. Journal of virology *77*, 9922-9930.

Pinton, P., Giorgi, C., Siviero, R., Zecchini, E., and Rizzuto, R. (2008). Calcium and apoptosis: ER-mitochondria Ca2+ transfer in the control of apoptosis. Oncogene *27*, 6407-6418.

Pinton, P., Rimessi, A., Romagnoli, A., Prandini, A., and Rizzuto, R. (2007). Biosensors for the detection of calcium and pH. Methods in cell biology *80*, 297-325.

Poiesz, B.J., Ruscetti, F.W., Gazdar, A.F., Bunn, P.A., Minna, J.D., and Gallo, R.C. (1980). Detection and isolation of type C retrovirus particles from fresh and cultured lymphocytes of a patient with cutaneous T-cell lymphoma. Proceedings of the National Academy of Sciences of the United States of America *77*, 7415-7419.

Proietti, F.A., Carneiro-Proietti, A.B., Catalan-Soares, B.C., and Murphy, E.L. (2005). Global epidemiology of HTLV-I infection and associated diseases. Oncogene *24*, 6058-6068.

Quintana, A., Griesemer, D., Schwarz, E.C., and Hoth, M. (2005). Calcium-dependent activation of T-lymphocytes. Pflugers Arch *450*, 1-12.

Quintana, A., Schwarz, E.C., Schwindling, C., Lipp, P., Kaestner, L., and Hoth, M. (2006). Sustained activity of calcium release-activated calcium channels requires translocation of mitochondria to the plasma membrane. The Journal of biological chemistry *281*, 40302-40309.

Quintana, A., Schwindling, C., Wenning, A.S., Becherer, U., Rettig, J., Schwarz, E.C., and Hoth, M. (2007). T cell activation requires mitochondrial translocation to the immunological synapse. Proceedings of the National Academy of Sciences of the United States of America *104*, 14418-14423.

Rahmani, Z., Huh, K.W., Lasher, R., and Siddiqui, A. (2000). Hepatitis B virus X protein colocalizes to mitochondria with a human voltage-dependent anion channel, HVDAC3, and alters its transmembrane potential. Journal of virology *74*, 2840-2846.

Rasola, A., and Bernardi, P. (2007). The mitochondrial permeability transition pore and its involvement in cell death and in disease pathogenesis. Apoptosis *12*, 815-833.

Rizzuto, R., Brini, M., Pizzo, P., Murgia, M., and Pozzan, T. (1995). Chimeric green fluorescent protein as a tool for visualizing subcellular organelles in living cells. Curr Biol *5*, 635-642.

Rizzuto, R., Pinton, P., Ferrari, D., Chami, M., Szabadkai, G., Magalhaes, P.J., Di Virgilio, F., and Pozzan, T. (2003). Calcium and apoptosis: facts and hypotheses. Oncogene *22*, 8619-8627.

Robek, M.D., Wong, F.H., and Ratner, L. (1998). Human T-cell leukemia virus type 1 pX-I and pX-II open reading frames are dispensable for the immortalization of primary lymphocytes. Journal of virology *72*, 4458-4462.

Rodgers, P.E. (1965). The Clinical Features and Aetiology of the Neuropathic Syndrome in Jamaica. The West Indian medical journal *14*, 36-47.

Rustin, P. (2002). Mitochondria, from cell death to proliferation. Nat Genet *30*, 352-353.

Sakai, A., Claire, M.S., Faulk, K., Govindarajan, S., Emerson, S.U., Purcell, R.H., and Bukh, J. (2003). The p7 polypeptide of hepatitis C virus is critical for infectivity and contains functionally important genotype-specific sequences. Proceedings of the National Academy of Sciences of the United States of America *100*, 11646-11651.

Sato, K., Maruyama, I., Maruyama, Y., Kitajima, I., Nakajima, Y., Higaki, M., Yamamoto, K., Miyasaka, N., Osame, M., and Nishioka, K. (1991). Arthritis in patients infected with human T lymphotropic virus type I. Clinical and immunopathologic features. Arthritis Rheum *34*, 714-721.

Satou, Y., Yasunaga, J., Yoshida, M., and Matsuoka, M. (2006). HTLV-I basic leucine zipper factor gene mRNA supports proliferation of adult T cell leukemia cells. Proceedings of the National Academy of Sciences of the United States of America *103*, 720-725.

Schwartz, S., Felber, B.K., Benko, D.M., Fenyo, E.M., and Pavlakis, G.N. (1990). Cloning and functional analysis of multiply spliced mRNA species of human immunodeficiency virus type 1. Journal of virology *64*, 2519-2529.

Shirakata, Y., and Koike, K. (2003). Hepatitis B virus X protein induces cell death by causing loss of mitochondrial membrane potential. The Journal of biological chemistry *278*, 22071-22078.

Shuh, M., and Derse, D. (2000). Ternary complex factors and cofactors are essential for human T-cell leukemia virus type 1 tax transactivation of the serum response element. Journal of virology *74*, 11394-11397.

Silic-Benussi, M., Cannizzaro, E., Venerando, A., Cavallari, I., Petronilli, V., La Rocca, N., Marin, O., Chieco-Bianchi, L., Di Lisa, F., D'Agostino, D.M., *et al.* (2009). Modulation of mitochondrial K(+) permeability and reactive oxygen species production by the p13 protein of human T-cell leukemia virus type 1. Biochimica et biophysica acta *1787*, 947-954.

Silic-Benussi, M., Cavallari, I., Zorzan, T., Rossi, E., Hiraragi, H., Rosato, A., Horie, K., Saggioro, D., Lairmore, M.D., Willems, L., *et al.* (2004). Suppression of tumor growth and cell proliferation by p13II, a mitochondrial protein of human T cell leukemia virus type 1. Proceedings of the National Academy of Sciences of the United States of America *101*, 6629-6634.

Sinha-Datta, U., Datta, A., Ghorbel, S., Dodon, M.D., and Nicot, C. (2007). Human T-cell lymphotrophic virus type I rex and p30 interactions govern the switch between virus latency and replication. The Journal of biological chemistry *282*, 14608-14615.

Siomi, H., Shida, H., Nam, S.H., Nosaka, T., Maki, M., and Hatanaka, M. (1988). Sequence requirements for nucleolar localization of human T cell leukemia virus type I pX protein, which regulates viral RNA processing. Cell *55*, 197-209.

Steinmann, E., Penin, F., Kallis, S., Patel, A.H., Bartenschlager, R., and Pietschmann, T. (2007). Hepatitis C virus p7 protein is crucial for assembly and release of infectious virions. PLoS pathogens *3*, e103.

Sun, S.C., and Yamaoka, S. (2005). Activation of NF-kappaB by HTLV-I and implications for cell transformation. Oncogene *24*, 5952-5964.

Szabadkai, G., Simoni, A.M., Bianchi, K., De Stefani, D., Leo, S., Wieckowski, M.R., and Rizzuto, R. (2006). Mitochondrial dynamics and Ca2+ signaling. Biochimica et biophysica acta *1763*, 442-449.

Tabakin-Fix, Y., Azran, I., Schavinky-Khrapunsky, Y., Levy, O., and Aboud, M. (2005). Functional inactivation of p53 by human T-cell leukemia virus type 1 Tax protein: mechanisms and clinical implications. Carcinogenesis.

Takada, S., Shirakata, Y., Kaneniwa, N., and Koike, K. (1999). Association of hepatitis B virus X protein with mitochondria causes mitochondrial aggregation at the nuclear periphery, leading to cell death. Oncogene *18*, 6965-6973.

Takeda, S., Maeda, M., Morikawa, S., Taniguchi, Y., Yasunaga, J., Nosaka, K., Tanaka, Y., and Matsuoka, M. (2004). Genetic and epigenetic inactivation of tax gene in adult T-cell leukemia cells. International journal of cancer *109*, 559-567.

Taylor, J.M., Ghorbel, S., and Nicot, C. (2009). Genome wide analysis of human genes transcriptionally and post-transcriptionally regulated by the HTLV-I protein p30. BMC genomics *10*, 311.

Thebault, S., Basbous, J., Hivin, P., Devaux, C., and Mesnard, J.M. (2004). HBZ interacts with JunD and stimulates its transcriptional activity. FEBS letters *562*, 165-170.

Toulza, F., Heaps, A., Tanaka, Y., Taylor, G.P., and Bangham, C.R. (2008). High frequency of CD4+FoxP3+ cells in HTLV-1 infection: inverse correlation with HTLV-1-specific CTL response. Blood *111*, 5047-5053.

Tsukasaki, K., Hermine, O., Bazarbachi, A., Ratner, L., Ramos, J.C., Harrington, W., Jr., O'Mahony, D., Janik, J.E., Bittencourt, A.L., Taylor, G.P., *et al.* (2009). Definition, prognostic factors, treatment, and response criteria of adult T-cell leukemia-lymphoma: a proposal from an international consensus meeting. J Clin Oncol *27*, 453-459.

Uchiyama, T., Yodoi, J., Sagawa, K., Takatsuki, K., and Uchino, H. (1977). Adult T-cell leukemia: clinical and hematologic features of 16 cases. Blood *50*, 481-492.

Verdonck, K., Gonzalez, E., Van Dooren, S., Vandamme, A.M., Vanham, G., and Gotuzzo, E. (2007). Human T-lymphotropic virus 1: recent knowledge about an ancient infection. The Lancet infectious diseases *7*, 266-281.

Xue, Y., Ren, J., Gao, X., Jin, C., Wen, L., and Yao, X. (2008). GPS 2.0, a tool to predict kinase-specific phosphorylation sites in hierarchy. Mol Cell Proteomics *7*, 1598-1608.

Yasunaga, J., and Matsuoka, M. (2007). Human T-cell leukemia virus type I induces adult T-cell leukemia: from clinical aspects to molecular mechanisms. Cancer Control *14*, 133-140.

Ye, J., Silverman, L., Lairmore, M.D., and Green, P.L. (2003). HTLV-1 Rex is required for viral spread and persistence in vivo but is dispensable for cellular immortalization in vitro. Blood *102*, 3963-3969.

Younis, I., and Green, P.L. (2005). The human T-cell leukemia virus Rex protein. Front Biosci *10*, 431-445.

Younis, I., Khair, L., Dundr, M., Lairmore, M.D., Franchini, G., and Green, P.L. (2004). Repression of human T-cell leukemia virus type 1 and type 2 replication by a viral mRNA-encoded posttranscriptional regulator. Journal of virology *78*, 11077-11083.

Zhang, W., Nisbet, J.W., Albrecht, B., Ding, W., Kashanchi, F., Bartoe, J.T., and Lairmore, M.D. (2001). Human T-lymphotropic virus type 1 p30(II) regulates gene transcription by binding CREB binding protein/p300. Journal of virology *75*, 9885-9895.

Zhang, W., Nisbet, J.W., Bartoe, J.T., Ding, W., and Lairmore, M.D. (2000). Human T-lymphotropic virus type 1 p30(II) functions as a transcription factor and differentially modulates CREB-responsive promoters. Journal of virology *74*, 11270-11277.

Zhao, T., Yasunaga, J., Satou, Y., Nakao, M., Takahashi, M., Fujii, M., and Matsuoka, M. (2009). Human T-cell leukemia virus type 1 bZIP factor selectively suppresses the classical pathway of NF-kappaB. Blood *113*, 2755-2764.

Zhou, Y., Frey, T.K., and Yang, J.J. (2009). Viral calciomics: interplays between Ca2+ and virus. Cell calcium *46*, 1-17.